Rates and Mechanisms for the Reactions of Chlorine Atoms with Iodoethane and 2-Iodopropane

John J. Orlando*

Atmospheric Chemistry Division, National Center for Atmospheric Research, Boulder, Colorado 80305

Charles A. Piety† and J. Michael Nicovich

School of Chemistry and Biochemistry, Georgia Institute of Technology, Atlanta, Georgia 30332

Michael L. McKee

Department of Chemistry and Biochemistry, Auburn University, Auburn, Alabama 36849

Paul H. Wine

School of Chemistry and Biochemistry and School of Earth and Atmospheric Sciences, Georgia Institute of Technology, Atlanta, Georgia 30332

Received: April 4, 2005; In Final Form: June 3, 2005

The reaction of Cl atoms with iodoethane has been studied via a combination of laser flash photolysis/resonance fluorescence (LFP−RF), environmental chamber/Fourier transform (FT)IR**,** and quantum chemical techniques. Above 330 K, the flash photolysis data indicate that the reaction proceeds predominantly via hydrogen abstraction. The following Arrhenius expressions (in units of cm^3 $molecule^{-1}$ s^{-1}) apply over the temperature range 334−434 K for reaction of Cl with CH_3CH_2I (k_4^H) and CD_3CD_2I (k_4^D): $k_4^H = (6.53 \pm 3.40) \times 10^{-11} \exp[-(428 \pm 206)/T]$ and $k_4^D = (2.21 \pm 0.44) \times 10^{-11} \exp[-(317 \pm 76)/T]$. At room temperature and below, the reaction proceeds both via hydrogen abstraction and via reversible formation of an iodoethane/Cl adduct. Analysis of the LFP−RF data yields a binding enthalpy (0 K) for $CD_3CD_2I{\cdot}Cl$ of 57 ± 10 kJ mol^{-1}. Calculations using density functional theory show that the adduct is characterized by a C−I−Cl bond angle of 84.5°; theoretical binding enthalpies of 38.2 kJ/mol, G2′[ECP(S)], and 59.0 kJ mol^{-1}, B3LYP/ECP, are reasonably consistent with the experimentally derived result. Product studies conducted in the environmental chamber show that hydrogen abstraction from both the $-CH_2I$ and $-CH_3$ groups occur to a significant extent and also provide evidence for a reaction of the $CH_3CH_2I{\cdot}Cl$ adduct with CH_3CH_2I, leading to CH_3CH_2Cl formation. Complementary environmental chamber studies of the reaction of Cl atoms with 2-iodopropane, CH_3CHICH_3, are also presented. As determined by relative rate methods, the reaction proceeds with an effective rate coefficient, k_6, of $(5.0 \pm 0.6) \times 10^{-11}$ cm^3 $molecule^{-1}$ s^{-1} at 298 K. Product studies indicate that this reaction also occurs via two abstraction channels (from the CH_3 groups and from the $-CHI-$ group) and via reversible adduct formation.

Introduction

The oceans provide the major source of iodine-containing organic compounds to the atmosphere.[1−3] While methyl iodide is the most abundant iodinated species present in the marine boundary layer,[4−10] other iodine-containing species have also been observed either in marine boundary layer air or in the ocean itself. These include multi-halogenated species (e.g., CH_2I_2, CH_2ICl) and also larger alkyl iodides including propyl and butyl iodides.[6,9,11,12] The gas-phase oxidation of these iodinated species, initiated by solar photolysis and reaction with OH and Cl atoms, results in the liberation of free iodine atoms. The inorganic iodine chemistry that ensues, which can also involve members of the HO_x and NO_x families, has been implicated in (1) the destruction of ozone in the marine boundary layer;[1,3,7] (2) the nucleation of particles in the marine boundary layer, with OIO likely playing a major role;[13−15] (3) the control of HO_2/OH and NO_2/NO ratios in the free troposphere;[7,16] and possibly (4) the destruction of ozone in the lower stratosphere (following convective transport of methyl iodide to this region).[16,17]

All iodine-containing organic compounds possess strong absorption features in the near-UV and are thus subject to rapid destruction via solar photolysis.[18−20] Photolysis lifetimes near the Earth's surface have been estimated to be about 2−3 days for methyl iodide and other simple alkyl iodides, while photolysis lifetimes for multi-halogenated species are considerably shorter (e.g., 5 min for CH_2I_2).

While photolysis likely represents the predominant gas-phase removal process for iodinated methanes in the atmosphere, larger alkyl iodides may also react with OH and Cl at a rate that is significant compared with their photolysis. For example, rate coefficients for reaction of OH with 1- and 2-iodopropane are about 20×10^{-13} and 15×10^{-13} cm^3 $molecule^{-1}$ s^{-1},

† Now at Department of Meteorology, University of Maryland, College Park, MD, 20742.

10.1021/jp051715x CCC: $30.25
Published on Web 07/13/2005

respectively,[21,22] implying partial atmospheric lifetimes for these species with respect to OH reaction of about 5−8 days. In addition, reactions of iodoethane and iodinated propanes and butanes with Cl atoms[23,24] have been shown to be sufficiently rapid to contribute to the atmospheric removal of these species, particularly in the marine boundary layer where Cl atom concentrations are likely elevated. For example, Cotter et al.[23] have reported a rate coefficient of 6.7×10^{-11} cm^3 molecule^{-1} s^{-1} for reaction of Cl with 1-iodopropane which, when combined with a marine boundary layer Cl atom concentration of perhaps 10^4 or even 10^5 atom cm^{-3},[25,26] implies that this process may be competitive.

However, the mechanisms for reactions of Cl with alkyl iodides appear to be complex, involving both abstraction and adduct-forming pathways,[24,27−32] and a quantitative understanding of these processes has yet to be obtained. The reaction that has been studied in the most detail is that of Cl atoms with methyl iodide,[23,24,27,28,31,32] for which both direct[23,27,32] and relative[28] kinetic data as well as product yield data[24,28,31] have been reported. Under tropospheric conditions, the reaction occurs both via a direct abstraction channel and via reversible adduct formation

$$Cl + CH_3I \rightarrow CH_2I + HCl \quad (1a)$$

$$Cl + CH_3I \leftrightarrow CH_3I{\cdot}Cl \quad (1b, -1b)$$

At 298 K and 1 atm pressure, the rate coefficient for adduct formation ($\sim 2 \times 10^{-11}$ cm^3 molecule^{-1} s^{-1})[27] is considerably larger than that for the abstraction reaction (10^{-12} cm^3 molecule^{-1} s^{-1}).[28] However, under these conditions, adduct formation is largely reversible ($k_{-1b} = 7000$ s^{-1}) and may thus have little impact under atmospheric conditions.[27] However, a modest increase in the effective rate coefficient, $k_{1,\mathrm{eff}}$, with total pressure and a positive dependence of the yield of CH_3Cl on the initial [CH_3I] provided evidence for the occurrence of other adduct loss processes[28,31]

$$CH_3I{\cdot}Cl \rightarrow \text{products} \quad (2)$$

$$CH_3I + CH_3I{\cdot}Cl \rightarrow CH_3Cl + \text{products} \quad (3)$$

The oxidation of iodoethane and 1- and 2-iodopropane by Cl atoms has been the subject of two studies by Cotter et al.[23,24]

$$Cl + CH_3CH_2I \rightarrow \text{products} \quad (4)$$

$$Cl + CH_3CH_2CH_2I \rightarrow \text{products} \quad (5)$$

$$Cl + CH_3CHICH_3 \rightarrow \text{products} \quad (6)$$

These authors report low-pressure rate coefficients for reactions 1, 4, 5, and 6,[23] obtained using a fast-flow discharge system, and also report end products for reactions 1, 4, and 6 in air at atmospheric pressure.[24] End-product analysis clearly shows the formation of carbonyl products (CH_3CHO from reaction 4 and acetone from reaction 6) that likely result from abstraction, for example

$$Cl + CH_3CH_2I \rightarrow CH_3CHI + HCl \quad (4a)$$

$$CH_3CHI + O_2 \rightarrow CH_3CHIOO^{\bullet} \quad (7)$$

$$2CH_3CHIOO^{\bullet} \rightarrow 2CH_3CHIO^{\bullet} + O_2 \quad (8a)$$

$$\rightarrow CH_3COI + CH_3CHIOH + O_2 \quad (8b)$$

$$CH_3CHIO^{\bullet} \rightarrow CH_3CHO + I \quad (9)$$

Cotter et al.[24] also report the formation of large yields of chloroalkanes that by analogy to reaction 3 might be adduct-related.

However, alkenes are possible products of the Cl atom initiated oxidation of either iodoethane or 2-iodopropane. In a recent study at NCAR,[33] a major product formed in the Cl atom initiated oxidation of bromoethane was ethene, which was postulated to originate from reaction of Cl at the methyl group in bromoethane, followed by decomposition of the resulting β-bromoalkyl radical

$$Cl + CH_3CH_2Br \rightarrow CH_2CH_2Br + HCl \quad (10)$$

$$CH_2CH_2Br \leftrightarrow CH_2CH_2 + Br \quad (11)$$

$$CH_2CH_2Br + O_2 \rightarrow O_2CH_2CH_2Br \quad (12)$$

An analogous mechanism has also been proposed for the formation of propene in the OH-initiated oxidation of 1-bromopropane.[34] Since the β-iodinated alkyl radicals, formed from abstraction at the methyl groups in iodoethane or 2-iodopropane, are likely to rapidly and irreversibly eliminate an iodine atom, for example

$$Cl + CH_3CH_2I \rightarrow CH_2CH_2I + HCl \quad (4b)$$

$$CH_2CH_2I \rightarrow CH_2{=}CH_2 + I \quad (13)$$

the formation of ethene (propene) in the case of iodoethane (2-iodopropane) seems likely.

In this paper, we present a thorough study of the reaction of Cl atoms with ethyl iodide, which includes time-resolved kinetic measurements obtained over a range of temperatures and pressures for both C_2H_5I and C_2D_5I, relative rate measurements obtained over a range of pressures (at 298 K) for C_2H_5I, and a quantum mechanical characterization of the Cl/ethyl iodide adduct. The combined data set shows clear evidence for the occurrence of adduct formation at atmospherically relevant temperatures, as well as for the occurrence of two abstraction pathways, reactions 4a and 4b. Complementary relative-rate and product studies of the Cl atom reaction with 2-iodopropane are also described.

Experimental Section

1. Georgia Tech Laser Flash Photolysis−Resonance Fluorescence System. Time-resolved chlorine atom kinetics in the presence of varying amounts of C_2H_5I or C_2D_5I were studied at Georgia Tech using the laser flash photolysis (LFP)−resonance fluorescence (RF) technique. The experimental apparatus was nearly identical to the one employed in previous studies of the reactions of atomic chlorine with CH_3I,[27] CH_2ICl,[30] and CH_3Br;[35] a schematic diagram of the apparatus is published elsewhere.[36] Important features of the experimental approach and details that are specific to this study are described below.

A jacketed Pyrex reaction cell with an internal volume of approximately 160 cm^3 was used in all experiments. The cell was maintained at a constant temperature by circulating ethylene glycol (for $T \geq 334$ K) or a 2:1 ethanol−methanol mixture (for $T \leq 305$ K) from a thermostated bath through the outer jacket. A copper−constantan thermocouple could be injected into the reaction zone through a vacuum seal, thus allowing measurement of the gas temperature under the precise pressure and flow rate conditions of the experiment. Temperature variation within the reaction volume (i.e., the volume from which fluorescence could

be detected) was found to be less than ±1 K under all experimental conditions employed in this study.

Chlorine atoms were produced by 355 nm laser flash photolysis of Cl_2

$$Cl_2 + h\nu\ (355\ nm) \rightarrow n Cl(^2P_{3/2}) + (2-n) Cl(^2P_{1/2}) \quad (14)$$

Third-harmonic radiation from a Quanta Ray Model DCR-2 Nd:YAG laser provided the photolytic light source. The photolysis laser could deliver up to 1×10^{17} photons per pulse at a repetition rate of up to 10 Hz; the third harmonic pulse width was ~6 ns. Fluences employed in this study ranged from 10 to 150 mJ cm^{-2} $pulse^{-1}$. The photolysis of Cl_2 at 355 nm is known to produce >99% ground-state $^2P_{3/2}$ atoms,[37,38] and for reasons discussed elsewhere,[27] it seems safe to assume that all Cl + iodoethane kinetic data reported in this study are representative of an equilibrium mixture of $Cl(^2P_{3/2})$ and $Cl(^2P_{1/2})$. As in earlier studies,[27,30,35] some experiments were carried out with CF_2Cl_2, a very efficient $Cl(^2P_{1/2})$ quencher,[39−41] added to the reaction mixture; in support of the hypothesis of spin−orbit state equilibration, this variation in experimental conditions had no effect on the observed kinetics.

To avoid the accumulation of photochemically generated reactive species, all experiments were carried out under "slow flow" conditions. The linear flow rate through the reactor was in the range 1.5−5.0 cm s^{-1}, while the laser repetition was either 5 or 10 Hz (10 Hz in most experiments). Since the direction of flow was perpendicular to the photolysis laser beam, no volume element of the reaction mixture was subjected to more than a few laser pulses.

Molecular chlorine (Cl_2), iodoethane, and CF_2Cl_2 flowed into the reaction cell from 12 L Pyrex bulbs containing mixtures in N_2 buffer gas, while N_2 flowed directly from its high-pressure storage tank; the bulb containing iodoethane was blackened to prevent photolysis by room lights. The gas mixtures were premixed upstream from the reaction cell. Concentrations of each component in the reaction mixture were determined from measurements of the appropriate mass flow rates and the total pressure. In addition, the fraction of iodoethane in the 12 L storage bulb was checked frequently by UV photometry at 254 nm using a mercury pen ray lamp as the light source. The absorption cross-sections needed to convert measured absorbances to concentrations were measured during the course of this study; in units of 10^{-19} cm^2 $molecule^{-1}$ (base e), the absorption cross-sections were found to be 12.8 for C_2H_5I and 13.3 for C_2D_5I. This C_2H_5I cross-section, believed to be accurate to within ±5%, is somewhat larger (10−15%) than values suggested by two spectra reported in the literature.[19,42]

The gases used in this study had the following stated minimum purities: N_2, 99.999%; Cl_2, 99.9%;[43] CF_2Cl_2, 99.9%.[43] Nitrogen was used as supplied, while Cl_2 and CF_2Cl_2 were degassed at 77 K before being used to prepare mixtures with N_2. The liquid C_2H_5I sample had a stated purity of 99%, while the isotopic purity of C_2D_5I was greater than 99.5%. The samples of C_2H_5I and C_2D_5I were transferred under nitrogen atmosphere into vials fitted with high-vacuum stopcocks and then degassed repeatedly at 77 K before being used to prepare mixtures with N_2.

2. NCAR Environmental Chamber. Relative-rate and product studies were carried out at NCAR in a 2-m-long, 47 L stainless steel environmental chamber, that has been described previously.[33,44,45] The chamber is interfaced to a Fourier transform (FT)IR spectrometer (Bomem DA3.01) via a set of Hanst-type multipass optics, which provide an observational path length of 32.6 m. Spectra were obtained using an MCT detector at a resolution of 1 cm^{-1} from the coaddition of 200 scans (acquisition time 3−4 min) and covered the range 800−3900 cm^{-1}. Photolyses were carried out along the length of the chamber, using the output of a Xe-arc lamp. For the vast majority of the experiments, the lamp output was restricted to the 300−400 nm range to avoid photolysis of the iodoalkanes. A few relative rate experiments, involving methanol as the reference compound, were conducted with a UV-enhanced lamp (filtered to cover the range 240−400 nm). In these experiments, small corrections (<5%) for photolytic loss of the iodoalkane were applied.

Rate coefficient measurements for reactions 4 and 6 were conducted using standard relative rate techniques, with CH_2O, CH_3OH, C_2H_5Cl (2-iodopropane only), C_2H_6 (iodoethane only), or CH_3CHO (iodoethane only) used as the reference compounds. Most measurements were made at 1 atm total pressure in either air or N_2 diluent, although a few determinations were made at 20−40 Torr total pressure in N_2. Typically, mixtures containing Cl_2 ($(3-6) \times 10^{15}$ molecule cm^{-3}), iodoethane or 2-iodopropane ($(2-28) \times 10^{14}$ molecule cm^{-3}), and one of the reference species ($(2-8) \times 10^{14}$ molecule cm^{-3}) were photolyzed for multiple periods ranging in duration from 30 s to 6 min, and an IR spectrum was recorded after each photolysis period. Decays of the iodoalkane and the reference species were monitored via IR absorption spectroscopy, and relative rate coefficients were obtained from the slopes of plots of the form given by equation A

$$\ln\{[\text{iodoalkane}]_0/[\text{iodoalkane}]_t\} = (k_{\text{iodoalkane}}/k_{\text{ref}})(\ln\{[\text{ref}]_0/[\text{ref}]_t\}) \quad (A)$$

where $k_{\text{iodoalkane}}$ and k_{ref} are the rate coefficients for Cl atom reaction with the iodoalkane and the reference species, and $[\text{iodoalkane}]_0$, $[\text{iodoalkane}]_t$, $[\text{ref}]_0$, and $[\text{ref}]_t$ refer to the concentrations of the iodoalkane and the reference compound at time zero and time t. Test experiments showed that heterogeneous losses of all compounds were of negligible (<5%) importance.

Products formed in the Cl atom initiated oxidation of iodoethane and 2-iodopropane were determined from multiple irradiations of mixtures of Cl_2 ($(2-10) \times 10^{15}$ molecule cm^{-3}) and the iodoalkane ($(3.5-56) \times 10^{14}$ molecule cm^{-3}) in 1 atm of N_2/O_2. An IR spectrum was recorded following each irradiation period, which ranged in duration from 3 to 5 min. Concentrations of most products (e.g., 2-chloropropane, acetone, propene, and chloroacetone from 2-iodopropane; chloroethane, acetaldehyde, formaldehyde, ethene, acetyl chloride, peracetic acid, CO, and CO_2 from iodoethane) in the photolyzed mixtures were determined via comparison with calibrated standard spectra measured in our laboratory. Chloroacetaldehyde, $ClCH_2CHO$, was quantified using IR absorption cross-sections reported by Yarwood et al.[46]

Trace constituents (Cl_2, the iodoalkanes, the reference compounds used in the relative rate studies) were added to the chamber from calibrated volumes (the contents of which were swept into the chamber with N_2), while O_2 was added directly to the chamber. The possible impact of iodoalkane dimerization[47] in the small (1 L) calibrated volume on the calculated iodoalkane pressures in the environmental chamber was investigated. Calibration curves (i.e., plots of IR absorbance in the chamber vs iodoalkane pressure in the calibrated volume) were linear for calibrated volume pressures as high as 5 Torr, indicating that no measurable amount of dimer was present in the calibrated volumes and thus that the iodoalkane partial

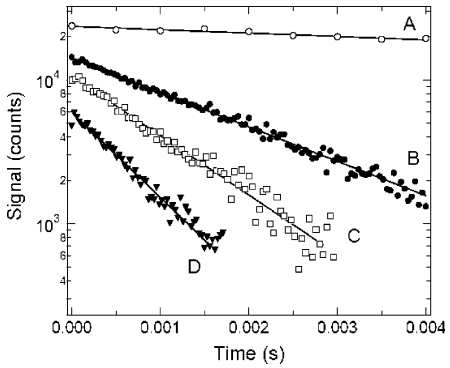

Figure 1. Typical Cl atom temporal profiles observed at $T \geq 334$ K. Reaction: Cl + C_2D_5I. Experimental conditions: $T = 395$ K; $P = 50$ Torr; $[Cl_2] = 4.1 \times 10^{12}$ per cm^3; $[Cl]_0 \approx 5 \times 10^{10}$ per cm^3; $[C_2D_5I]$ in units of 10^{13} per cm^3 = (A) 0, (B) 5.64, (C) 10.2, (D) 13.7. Solid lines are obtained from least-squares analyses and give the following pseudo-first-order decay rates in units of s^{-1}: (A) 39, (B) 568, (C) 1023, (D) 1436. For the sake of clarity, traces B, C, and D are scaled upward by factors of 1.8, 1.5, and 1.4, respectively.

pressure in the chamber could be accurately determined from the ratio of the cell volume to the calibrated volume.

Chemicals used in these experiments were obtained from the following sources: Cl_2 (Matheson, UHP); iodoethane, 2-iodopropane, chloroethane, acetaldehyde (all Aldrich, >99+%); methanol (Mallinckrodt, HPLC grade); ethane (Matheson, C. P. Grade); O_2 (U. S. Welding); N_2, (boil-off from liquid N_2, U. S. Welding). Gaseous formaldehyde was obtained by heating paraformaldehyde (Eastman Organic Chemicals) under vacuum. Gases (chloroethane, ethane) were used as received, while liquids (iodoethane, 2-iodopropane, acetaldehyde, and methanol) were subjected to several freeze−pump−thaw cycles before use.

Results and Discussion

1. Reaction of Cl Atoms with Iodoethane. *A. LFP−RF Studies at $T \geq 334$ K.* All LFP−RF studies were carried out under pseudo-first-order conditions with iodoethane in large excess (factors of 50−5000) over Cl. Hence, in the absence of side reactions that remove or produce chlorine atoms, the Cl temporal profile following the laser flash would be described by the relationship

$$\ln\{[Cl]_0/[Cl]_t\} = (k_4[\text{iodoethane}] + k_{15})t = k't \qquad \text{(B)}$$

where k_{15} is the rate coefficient for the reaction

Cl → first-order loss by diffusion from the detector field of view and/or reaction with background impurities. (15)

The bimolecular rate coefficients of interest, $k_4(P, T)$, are determined from the slopes of k' versus [iodoethane] plots for data obtained at constant T and P. Observance of Cl temporal profiles that are exponential (i.e., obey eq B), a linear dependence of k' on [iodoethane] and invariance of k' to variation in laser photon fluence and photolyte (Cl_2) concentration, strongly suggest that reactions 4 and 15 are, indeed, the only processes that significantly affect the Cl time history.

For all experiments carried out at temperatures of 334 K and above, well-behaved pseudo-first-order kinetics were observed, that is, Cl atom temporal profiles were well-described by eq B, and observed k' values increased linearly with increasing [iodoethane] but were independent of laser photon fluence and photolyte concentration. Typical data are shown in Figures 1 and 2, while measured bimolecular rate coefficients, $k_4(T)$, for both C_2H_5I (k_4^H) and C_2D_5I (k_4^D) reactants, are summarized in

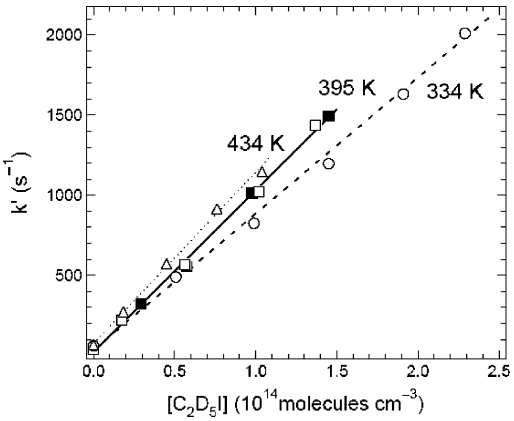

Figure 2. Plots of k', the pseudo-first-order Cl atom decay rate, vs C_2D_5I concentration for data at three different temperatures. The 334 K data were obtained at $P = 205$ Torr, while the 395 and 434 K data were obtained at $P = 50$ Torr. The filled squares are 395 K data points obtained with CF_2Cl_2 added to provide more efficient equilibration of the Cl spin−orbit states. The lines are obtained from least-squares analyses; their slopes give the rate coefficients summarized in Table 1.

TABLE 1: Summary of LFP−RF Kinetic Data for Reactions of Cl with Iodoethane and Deuterated Iodoethane at Temperatures in the Range 334−434 K

T^a	P^a	$[Cl_2]$	$[Cl]_0$	no. of expts.^{b}	$[\text{iodoethane}]_{max}$	k'_{max} ^{a}	k_4 ^{a,c}
				Cl + CH_3CH_2I			
350	50	71	0.62	4	1160	2310	19.5 ± 0.2
395	50	120	0.70−2.0	5	1090	2500	22.7 ± 1.3^d
395	50	90	0.65	3	381	902	22.6 ± 2.6
396	20	69	1.9	3	1130	2420	20.5 ± 1.2^d
396	20	69	1.9	3	1120	2500	21.5 ± 3.5
434	50	68	1.2	6	1170	2960	24.7 ± 0.7
				Cl + CD_3CD_2I			
334	20	67	1.0	6	2270	2120	9.01 ± 0.65
334	205	100	1.8	6	2290	2010	8.40 ± 0.50
350	50	52	0.50	6	1960	1780	8.67 ± 0.70
366	50	57	0.96	6	1580	1490	9.12 ± 0.19
380	50	60	1.0	6	3920	3560	9.03 ± 0.26
395	50	120	1.0	5	1450	1490	10.1 ± 0.5^d
395	50	41	0.50	5	1370	1440	10.0 ± 0.5
396	20	70	2.0	3	2070	2190	10.1 ± 0.2^d
396	20	70	2.0	3	2070	2060	9.50 ± 0.76
416	50	58	0.95	4	7710	8060	10.3 ± 0.2
434	50	69	0.92	5	1010	1140	10.7 ± 0.4

^{a} Units: T (K); P (Torr); concentrations (10^{11} molecules cm^{-3}); k' (s^{-1}); k_4(10^{-12} cm^3 molecule^{-1} s^{-1}). ^{b} Expt. ≡ measurement of one pseudo-first-order decay rate. ^{c} Uncertainties are 2σ and represent precision only. ^{d} 0.5 Torr CF_2Cl_2 added to the reaction mixture to speed up equilibration of the atomic chlorine spin−orbit states.

Table 1. At 334 K, k_4^D is found to be independent of pressure over the range 20−205 Torr, while at 395−396 K, both k_4^H and k_4^D are essentially independent of pressure over the range 20−50 Torr. Arrhenius plots for the reactions of Cl with C_2H_5I and C_2D_5I are shown in Figure 3. The solid lines in Figure 3 are obtained from linear least-squares analyses of the ln k_4 vs T^{-1} data that give the following Arrhenius expressions

$$k_4^H = (6.53 \pm 3.40) \times 10^{-11} \exp[-(428 \pm 206)/T] \text{ cm}^3 \text{ molecule}^{-1} \text{ s}^{-1} \qquad \text{(C)}$$

$$k_4^D = (2.21 \pm 0.44) \times 10^{-11} \exp[-(317 \pm 76)/T] \text{ cm}^3 \text{ molecule}^{-1} \text{ s}^{-1} \qquad \text{(D)}$$

Uncertainties in the above Arrhenius expressions are 2σ and

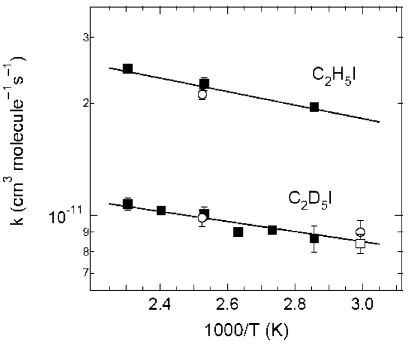

Figure 3. Arrhenius plots for the reactions of Cl with C_2H_5I and C_2D_5I at $T \geq 334$ K. The open circles, filled squares, and open squares represent data obtained at pressures of 20, 50, and 205 Torr, respectively.

refer to the precision of the Arrhenius parameters. As summarized in Table 1, the 2σ precision of individual rate coefficients is typically about 5%. Uncertainties in iodoethane concentrations represent the dominant source of systematic error in the rate coefficient determinations. Complications from impurity reactions and secondary reactions, which are discussed in a later section, are thought to be a very minor source of systematic error. We estimate the absolute accuracy of the reported rate coefficients to be ±25% independent of temperature; this uncertainty will be reduced substantially when differences in reported iodoethane UV absorption cross-sections are resolved. The significant observed kinetic isotope effect (more than a factor of 2 at all temperatures in the range 334−434 K) suggests that the dominant reaction mechanism is hydrogen abstraction (i.e., for the temperatures and iodoethane concentrations employed to obtain the data summarized in Table 1, $k_4 \approx k_{4a} + k_{4b}$). The NCAR product studies that are reported in a later section provide strong support for the hydrogen abstraction mechanism and also provide estimates of the relative importance of the two hydrogen abstraction channels (i.e., abstraction of an α- or β-hydrogen).

B. LFP−RF Studies at 256 K ≤ T ≤ 305 K. Over the temperature range 256−305 K, initial chlorine atom decay rates were considerably faster than expected on the basis of extrapolation of the high-temperature results (see above), and chlorine atom regeneration via a secondary reaction became evident. Under these experimental conditions, observed Cl atom temporal profiles were independent of laser fluence and $[Cl_2]$ but varied as a function of [iodoethane], pressure, and temperature in the manner expected if formation and unimolecular decomposition of an iodoethane−Cl adduct was the source of both enhanced reactivity at early times after the laser flash and regenerated chlorine atoms. Reported below is a data set that was obtained with the goal of quantifying the kinetics of adduct formation and dissociation and, therefore, obtaining information about adduct thermochemistry. Addition of Cl to the iodine atom is expected to occur with the same rate coefficient for C_2H_5I and C_2D_5I, and differences in the equilibrium constants for adduct formation/dissociation between the deuterated and undeuterated reactants can be readily evaluated using statistical thermodynamics. However, the slower D-abstraction rate coefficient for C_2D_5I is a significant advantage for obtaining quantitative experimental determinations of k_{4c} and k_{-4c}.

$$Cl + C_2D_5I + N_2 \leftrightarrow C_2D_5I{\cdot}Cl + N_2 \qquad (4c, -4c)$$

Hence, the results described below were all obtained using C_2D_5I as the iodoethane reactant.

Assuming that $C_2D_5I{\cdot}Cl$ decomposition is the source of regenerated Cl atoms, the relevant kinetic scheme controlling the Cl temporal profile includes reactions 4a, 4b, 4c, −4c, 15, and 16.

$$C_2D_5I{\cdot}Cl \rightarrow \text{first-order loss by processes that do not regenerate Cl atoms} \qquad (16)$$

Assuming that all processes affecting the temporal evolution of Cl and $C_2D_5I{\cdot}Cl$ are first-order or pseudo-first-order, the rate equations for the above reaction scheme can be solved analytically

$$S_t/S_0 = [(Q + a_1)\exp(a_1 t) - (Q + a_2)\exp(a_2 t)]/(a_1 - a_2) \qquad (E)$$

where S_t and S_0 are the resonance fluorescence signal levels at times t and 0, and

$$Q = k_{-4c}{}^{D} + k_{16} \qquad (F)$$

$$Q + k_{15} + k_4{}^{D}[C_2D_5I] = -(a_1 + a_2) \qquad (G)$$

$$Q\{k_{15} + (k_{4a}{}^{D} + k_{4b}{}^{D})[C_2D_5I]\} + k_{16}k_{4c}{}^{D}[C_2D_5I] = a_1a_2 \qquad (H)$$

In eq G, $k_4{}^{D} = k_{4a}{}^{D} + k_{4b}{}^{D} + k_{4c}{}^{D}$.

Observed Cl atom temporal profiles were fit to the double exponential eq E to obtain values for a_1, a_2, Q, and S_0. The background Cl loss rate in the absence of C_2D_5I (i.e., k_{15}) was directly measured at each temperature and pressure, and rate coefficients for hydrogen abstraction (i.e., $k_{4a}{}^{D} + k_{4b}{}^{D}$) were obtained by extrapolation of the high-temperature data using eq D. Rearrangement of the above equations shows that the rate coefficients $k_{4c}{}^{D}$, $k_{-4c}{}^{D}$, and k_{16} can be obtained from the fit parameters and the experimental values for k_{15} and $k_{4a}{}^{D} + k_{4b}{}^{D}$ as follows

$$k_{4c}{}^{D} = -\{Q + k_{15} + (k_{4a}{}^{D} + k_{4b}{}^{D})[C_2D_5I] + a_1 + a_2\}/[C_2D_5I] \qquad (I)$$

$$k_{16} = \{a_1a_2 - Q(k_{15} + (k_{4a}{}^{D} + k_{4b}{}^{D})[C_2D_5I])\}/(k_{4c}{}^{D}[C_2D_5I]) \qquad (J)$$

$$k_{-4c}{}^{D} = Q - k_{16} \qquad (K)$$

Typical chlorine atom temporal profiles observed in the experiments at $T = 256-305$ K are shown in Figure 4 along with the best fits of each temporal profile to eq E; the results for all experiments in this temperature range are summarized in Table 2. Inspection of Table 2 shows that the derived values for $k_{4c}{}^{D}$ and $k_{-4c}{}^{D}$ vary in a sensible way as a function of temperature and pressure, that is, both rate coefficients increase with increasing pressure, $k_{-4c}{}^{D}$ increases dramatically with increasing temperature, and $k_{4c}{}^{D}$ decreases slightly with increasing temperature. Comparison of rate coefficients derived from multiple measurements at a particular temperature and pressure shows that the precision of derived values is excellent for $k_{4c}{}^{D}$, but not as good for $k_{-4c}{}^{D}$. We estimate that the accuracy of derived rate coefficients is ±25% for $k_{4c}{}^{D}(P, T)$ and ±35% for $k_{-4c}{}^{D}(P, T)$ over the full range of temperature and pressure spanned by the results in Table 2.

C. Secondary Chemistry Complications in the LFP−RF Studies. The photochemical system used in the LFP−RF studies of reaction 4 is believed to be relatively free of complications

TABLE 2: Results of the Cl + C_2D_5I + N_2 ↔ C_2D_5I·Cl + N_2 Equilibration Kinetics Experiments[a]

T	P	$[Cl_2]$	$[Cl]_0$	$[C_2D_5I]$	Q	$-a_1$	$-a_2$	k_{15}	k_{16}	$k_{-4c}{}^D$	$k_{4c}{}^D$	K_P
256	260	126	2.1	232	431	94.1	2970	38	81	350	105	861
256	260	70	1.2	150	347	62.9	1900	38	49	298	98.8	951
256	260	83	1.4	71.5	322	58.1	1050	38	49	273	98.8	1040
256	260	69	1.1	22.2	273	45.1	489	38	37	235	94.6	1150
268	270	83	1.5	475	794	56.8	5170	80	−6	800	84.8	291
268	270	86	1.5	320	944	113	3800	80	52	941	82.1	239
268	270	83	1.5	240	886	96.4	3110	80	41	844	86.9	283
268	270	85	1.5	131	913	109	2080	80	67	847	85.1	276
276	280	76	1.5	2270	1930	149	23800	80	16	1910	89.6	124
276	280	77	1.6	1920	2360	303	21000	80	172	2190	91.4	111
276	280	82	1.4	946	1750	86.5	10300	80	−52	1800	83.5	123
276	280	82	1.4	308	1950	141	4880	80	40	1910	90.2	126
285	80	53	0.8	1840	2960	274	14300	106	−34	3000	55.3	47.5
285	80	52	0.8	830	2670	216	7790	106	−45	2720	55.8	52.9
285	80	53	0.8	411	2850	209	5350	106	−15	2870	55.9	50.2
286	287	80	1.4	2310	4960	415	25600	106	91	4870	83.4	44.0
286	287	79	1.5	1290	4720	327	15800	106	21	4700	80.0	43.7
286	287	77	1.3	542	4870	249	9550	106	−15	4890	81.6	42.8
298	300	59	1.4	2880	11900	825	34700	57	90	11800	74.3	15.5
298	300	55	1.5	2250	10400	667	28000	57	12	10400	73.1	17.3
298	300	56	1.4	1530	10800	613	22100	57	38	10800	70.2	16.1
298	300	59	1.4	547	10900	367	14900	57	84	10800	71.9	16.4
305	50	68	0.9	2590	11400	1010	22900	50	−42	11500	40.2	8.44
305	50	62	0.9	2100	11100	952	19600	50	−6	11100	37.1	8.03
305	300	105	1.4	3840	32100	1300	74200	50	−31	32200	105	7.84
305	300	106	1.2	2640	36900	1190	69200	50	147	36800	119	7.77

[a] Units: T (K); P (Torr); concentrations (10^{11} per cm^3); Q, a_1, a_2, k_{15}, k_{16}, $k_{-4c}{}^D$ (s^{-1}); k_{4c} (10^{-12} cm^3 molecule^{-1} s^{-1}); K_P (10^4 atm^{-1}). [b] 0.5 Torr CF_2Cl_2 added to speed up equilibration of the atomic chlorine spin−orbit states.

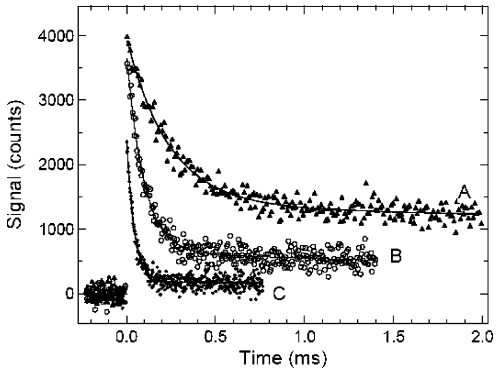

Figure 4. Typical Cl atom temporal profiles observed at 256 K ≤ T ≤ 305 K. Experimental conditions: T = 276 K; P = 280 Torr; $[Cl_2]$ = 8.0 × 10^{12} per cm^3; $[Cl]_0 \approx 1.4 \times 10^{11}$ per cm^3; $[C_2D_5I]$ in units of 10^{13} per cm^3 = (A) 3.08, (B) 9.46, (C) 22.7. Solid lines are obtained from nonlinear least-squares fits to eq E. Best fit parameters in units of s^{-1}: Q = (A) 1950, (B) 1750, (C) 1930; $-a_1$ = (A) 141, (B) 86.5, (C) 149; $-a_2$ = (A) 4880, (B) 10 300, (C) 23 800.

from unwanted side reactions. Radical concentrations were kept low enough, (0.5−2.1) × 10^{11} molecule cm^{-3}, that consumption of Cl or C_2D_5I·Cl via radical−radical reactions can be ruled out. Furthermore, the reactions of Cl with iodoethane are fast enough that minor impurities in the iodoethane samples could not compete effectively for Cl atoms. To avoid generation of high radical concentrations via iodoethane photolysis, Cl atoms were generated by photodissociation of Cl_2 at 355 nm, a wavelength where the iodoethane absorption cross-section is negligible ($\sigma_{355} = 3 \times 10^{-23}$ cm^2 molecule^{-1}).[19] Use of Cl_2 as the photolyte does, however, result in the possibility that Cl can be regenerated via the following secondary reaction (and the analogous reaction involving CD_3CDI)

$$CH_3CHI + Cl_2 \rightarrow CH_3CHICl + Cl \qquad (17)$$

To our knowledge, no kinetic data for reaction 17 are reported in the literature. However, rate coefficients for the reactions of CH_2I, CH_2Cl, and CH_3CHCl with Cl_2, in units of 10^{-13} cm^3 molecule^{-1} s^{-1}, are reported to be 11.5 exp(−96/T),[48] 15.1 exp(−493/T),[48] and 43.7 at 298 K,[49] respectively. On the basis of the above literature values, it seems likely that k_{17} is less than 1×10^{-11} cm^3 molecule^{-1} s^{-1} over the entire temperature and pressure regime of this study. To examine the magnitude of possible kinetic interference from reaction 17, we have carried out numerical simulations of the reaction kinetics, assuming a Cl_2 concentration of 1.2×10^{13} molecules cm^{-3} (i.e., the highest concentration employed in any of the experiments summarized in Table 1). On the basis of product studies that are discussed in a later section, the CH_3CHI and CD_3CDI yields from the Cl + iodoethane reaction assumed in the simulations were 0.67. The simulations indicate that the occurrence of reaction 17 with a rate coefficient of 1×10^{-11} cm^3 molecule^{-1} s^{-1} would result in slightly nonexponential decays which, if fit to an exponential function over three e-folding times, would lead to underestimation of the Cl + C_2H_5I rate coefficient by about 5%. We have carefully examined the data with the highest Cl_2 concentrations (i.e., the experiments at T = 395 K and P = 50 Torr with CF_2Cl_2 added (see Table 1)), and we find no evidence for nonexponential decays; essentially identical decay rates are obtained if the data are analyzed over 1, 2, or 3 e-folding times. We conclude that the high-temperature LFP−RF kinetic data are unaffected by interference from Cl regeneration via reaction 17. As confirmed by simulations, the observed kinetics of the approach to equilibrium between Cl and C_2D_5I·Cl are also unaffected by the occurrence of reaction 17, because Cl regeneration by this reaction is much slower than Cl regeneration via adduct decomposition under all experimental conditions employed.

D. C_2D_5I·Cl Thermochemistry. The equilibrium constants (K_P) given in Table 2 are computed from the relationship

$$K_P = k_{4c}{}^D/(k_{-4c}{}^D RT) = K_C/RT \qquad (L)$$

A plot of ln K_P vs 1/T (i.e., a van't Hoff plot) is shown in Figure

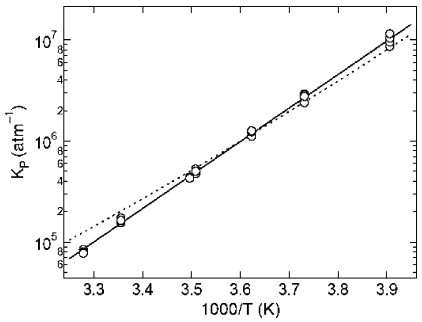

Figure 5. van't Hoff plot for the reaction Cl + $C_2D_5I \leftrightarrow C_2D_5I{\cdot}Cl$. The solid line is obtained from a least-squares analysis and gives the second law thermochemical parameters for the reaction (see text and Table 4). The dashed line is based on the third law analysis.

5. The enthalpy and entropy changes associated with reaction 4c are obtained from the slope and intercept of the van't Hoff plot (solid line in Figure 5) via the relationship

$$\ln K_P = (\Delta S/R) - (\Delta H/RT) \qquad \text{(M)}$$

At 278 K, the midpoint of the experimental $1/T$ range, this "second law analysis" gives the results $\Delta H = -63.4 \pm 2.4$ kJ mol^{-1} and $\Delta S = -113.5 \pm 8.5$ J K^{-1} mol^{-1}; the reported uncertainties are 2σ and represent the precision of the ln K_P vs $1/T$ data only.

In addition to the second law analysis described above, we have also carried out a third law analysis, where the experimental value of K_P at 278 K, $(9.6 \pm 2.0) \times 10^5$ atm^{-1}, has been employed in conjunction with a calculated entropy change to determine ΔH.

Since experimental data concerning the structure of $C_2D_5I{\cdot}$Cl are not available, electronic structure calculations have been carried out for this species and also for C_2D_5I. All calculations were made with *Gaussian 03*.[50] Optimized geometries were determined using density functional theory (DFT)[51] with the B3LYP exchange/correlation functional. A 6-311+G(d,p) basis set was used for carbon and hydrogen, while an effective core potential[52] (ECP) was used for the core electrons of iodine in conjunction with an uncontracted 5s5p1d basis set for the valence orbitals. This level of theory is denoted B3LYP/ECP.

Recently, the G2[53] and G2(MP2)[54] levels of theory have been extended to include iodine.[55] Both levels of theory approximate results from the QCISD(T)/6-311+G(3df,2p) level with zero-point and higher-level corrections. The computational method includes all-electron calculations (AE) for all atoms except iodine where an effective core potential (ECP(S = Stuttgart)) was used. In the G2 computational scheme for iodine, a 11111/11111/1 contraction is used for the valence orbitals in place of the 6-311+G(d,p) basis set, and a 11111/11111/111/1 contraction is used in place of the 6-311+G(3df,2p) basis set. The mean absolute deviations from experiment at the G2[ECP(S)] level for iodine-containing molecules of ionization energies, electron affinities, and atomization energies is only 10 kJ mol^{-1}.

In this study, we have followed the G2[ECP(S)] prescription with the exception that we use B3LYP/ECP geometries and corresponding vibrational frequencies (with no scaling factor) rather than the MP2/ECP geometry and HF/ECP frequencies (with 0.893 scaling factor). A spin−orbit correction to the binding enthalpy is made for the chlorine atom (3.5 kJ mol^{-1}). We use the notation G2′[ECP(S)] to denote these differences. The B3LYP/ECP geometries are compared in Figure 6 for ICH_2-CH_3 and $Cl{\cdot}ICH_2CH_3$. This adduct structure is essentially identical to that recently reported by Enami et al.[32] These authors also identify a cis isomer of the adduct, 3.8 kJ mol^{-1} higher in energy, possessing an imaginary frequency. It is possible that this cis structure is the transition state to pathway 4b, abstraction of a hydrogen from the methyl group in iodoethane.

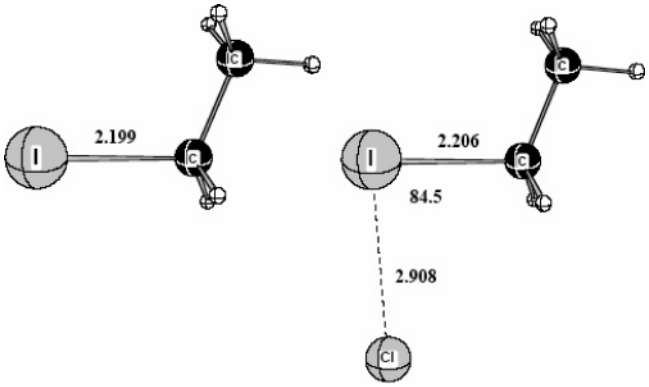

Figure 6. Structures for C_2H_5I and $C_2H_5I{\cdot}Cl$ derived from electronic structure calculations at the B3LYP/ECP level.

TABLE 3: Summary of Parameters Used in Calculations of Absolute Entropies and Heat Capacity Corrections

	Cl	C_2D_5I	$C_2D_5I{\cdot}Cl$
g_0	4	1	2
g_1	2		
$\Delta\epsilon$ (cm^{-1})[a]	882.36		
rotational		0.6456	0.1117
constants (cm^{-1})		0.08062	0.04762
		0.07575	0.03426
I_r (amu Å^2)			88[b]
ν (cm^{-1})		183, 226, 444, 554, 727, 745, 903, 979, 984, 1067, 1071, 1088, 1167, 2172, 2254, 2282, 2309, 2354	22[c], 61, 164, 183, 226, 434, 559, 732, 746, 900, 976, 980, 1067, 1069, 1088, 1171, 2175, 2263, 2284, 2310, 2368

[a] $\Delta\epsilon \equiv$ energy splitting between the two lowest electronic states. Only Cl has an excited electronic state that is low enough in energy to contribute to the entropy. [b] Estimated moment of inertia for the internal rotation of C_2D_5 about ICl.[58] [c] This is the frequency for the internal rotation of C_2D_5 about ICl; this motion was treated as a free rotation (see text).

To carry out the third law analysis, the absolute entropy of Cl as a function of temperature was obtained from the JANAF tables,[56] while the absolute entropies for C_2D_5I and $C_2D_5I{\cdot}Cl$ were calculated using the results of the electronic structure calculations described above. The assumed vibrational frequencies and moments of inertia are given in Table 3. The lowest-frequency normal mode for $C_2D_5I{\cdot}Cl$ (frequency = 22 cm^{-1}) is the internal rotation of the ethyl group around ICl. Some additional calculations, carried out to assess the magnitude of the internal rotation barriers, suggest that the barriers for methyl rotations are large enough (∼12 kJ mol^{-1}) that these torsions should be treated as vibrations in the entropy calculations. However, the barrier for rotation of C_2D_5 around ICl is calculated to be only 0.5 kJ mol^{-1}; hence, the 22 cm^{-1} normal mode "vibration" was treated as a free rotation in the entropy calculations. At 278 K, the third law analysis gives the results $\Delta H = -53.2 \pm 4.0$ kJ mol^{-1} and $\Delta S = -77.0 \pm 8.0$ J K^{-1} mol^{-1}; the uncertainties we report reflect an estimate of our imperfect knowledge of the input data needed to calculate absolute entropies (the low-frequency vibrations of $C_2D_5I{\cdot}Cl$ are most significant) as well as the estimated uncertainty in the experimental value for K_P (278 K). Treating the 22 cm^{-1} adduct

TABLE 4: Thermochemical Parameters for the Reaction Cl + $C_2D_5I \rightarrow C_2D_5I \cdot Cl$

T (K)	method	$-\Delta_r H$ (kJ mol^{-1})[a]	$-\Delta_r S$ (J K^{-1} mol^{-1})[a]
298	2nd law	63.4 ± 4.0	114 ± 15
	3rd law	53.3 ± 4.0	77 ± 8
278	2nd law	63.4 ± 4.0	114 ± 15
	3rd law	53.3 ± 4.0	77 ± 8
0	2nd law	62.2 ± 4.5	0.0
	3rd law	52.0 ± 4.5	0.0

[a] Uncertainties are accuracy estimates at the 95% confidence level.

mode as a vibration would, for example, change the calculated entropy change from −77.0 to −88.2 J K^{-1} mol^{-1}.

The thermochemical results obtained in this study are summarized in Table 4. Appropriate heat capacity corrections have been employed to obtain ΔH values at 298 and 0 K. As can be seen from Table 4, the agreement between the second and third law results is far from perfect. The dashed line in Figure 5 is a plot of ln K_P vs T^{-1} that is based on the third law analysis. It can be seen that a relatively small temperature-dependent systematic error in the measured equilibrium constants could potentially account for the difference between the solid and dashed lines in Figure 5. While the source, or even the existence, of such a systematic error cannot be identified with any degree of certainty, it is worth noting that extraction of equilibrium constants from the experimental data required estimation of the fraction of Cl loss attributable to hydrogen transfer. Extrapolation of the high-temperature data assuming Arrhenius behavior was employed to evaluate the H-transfer rate coefficient. The accuracy of this procedure is somewhat questionable, particularly since the product studies discussed below indicate that two different H-transfer pathways, which may have different activation energies, are important. It should be noted, however, that the extrapolated 298 K value for $k_{4a}^H + k_{4b}^H$ agrees quantitatively with the 298 K value for k_4^H in 1.5−5.0 Torr He reported by Cotter et al.[23]

Since uncertainties in the second and third law values for ΔH are similar, it seems appropriate to report averages of the second and third law values, while adjusting reported uncertainties to encompass the 2σ error limits of both determinations. Using this approach, we report the following ΔH values for the Cl + C_2D_5I association reaction: −58 ± 9 kJ mol^{-1} at 298 K and −57 ± 10 kJ mol^{-1} at 0 K.

The theoretical binding enthalpy (0 K) of $Cl \cdot ICH_2CH_3$ is found to be 38.2 and 59.0 kJ mol^{-1} by G2′[ECP(S)] and B3LYP/ECP, respectively. The B3LYP/ECP value compares well with that of Enami et al.,[32] 61.7 kJ mol^{-1}, using a similar level of theory. Our $Cl \cdot ICH_2CH_3$ values are slightly smaller than the binding enthalpies computed for $Cl \cdot ICH_3$, 40.0 and 59.3 kJ mol^{-1}, using similar levels of theory.[27] On the other hand, the experimental binding enthalpy of 57 ± 10 kJ mol^{-1} (for $Cl \cdot ICD_2CD_3$) is slightly larger than the experimental $Cl \cdot ICH_3$ binding enthalpy of 52 ± 3 kJ mol^{-1},[27] although the experimental results are equal within the reported uncertainties. It is known that DFT has a particular problem with 2c−3e bonds, particularly with unsymmetrical 2c−3e bonds, because spin is excessively delocalized.[57] Lower-level wave function methods such as MP2 can also fail to correctly describe 2c−3e bonding because of excessive spin localization. On the basis of experience with similar systems,[27,35] we expected the true binding enthalpy to be bracketed between the G2′ and DFT values. In this case, however, the experimental value is very close to the DFT result.

E. Relative Rate Determinations. The rate coefficient for reaction of Cl atoms with iodoethane, k_4, was determined at 298 K in the NCAR environmental chamber using the relative rate technique, with formaldehyde, ethane, acetaldehyde, and methanol employed as reference compounds

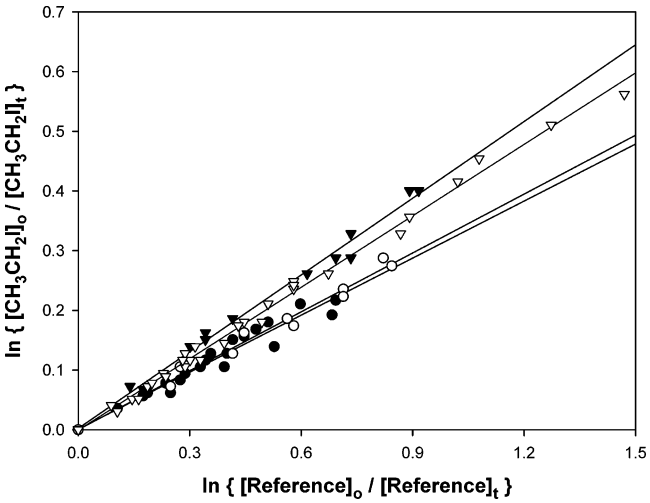

Figure 7. Relative rates of decay of CH_3CH_2I vs C_2H_6 (solid triangles, 720 Torr air), vs CH_3CHO (open circles, 30 Torr N_2), vs CH_3OH (open triangles, 720 Torr air), and vs CH_2O (solid circles, 720 Torr N_2) in the presence of Cl atoms.

$$Cl + CH_3CH_2I \rightarrow \text{products} \quad (4)$$

$$Cl + CH_2O \rightarrow HCO + HCl \quad (18)$$

$$Cl + CH_3OH \rightarrow CH_2OH + HCl \quad (19)$$

$$Cl + CH_3CHO \rightarrow CH_3CO + HCl \quad (20)$$

$$Cl + CH_3CH_3 \rightarrow CH_3CH_2 + HCl \quad (21)$$

Data for CH_2O and CH_3CHO were obtained in N_2 diluent only (30 and 720 Torr total pressure), since these two compounds are products of iodoethane oxidation in air. Studies using ethane as the reference were conducted in 720 Torr air, while methanol data were obtained in both N_2 and air diluent (720 Torr total pressure in both cases). In all cases, multiple runs were carried out with the $[CH_3CH_2I]$/[reference] ratio varied by at least a factor of 2. In some cases (with CH_2O as reference, 720 Torr N_2; with methanol as reference, 720 Torr air; and with ethane as reference, 720 Torr air), the $[CH_3CH_2I]$, as well as the $[CH_3CH_2I]$/[reference] ratio, was varied by a factor of at least 8. No variation of the rate coefficient for reaction 4 was observed in any case.

Representative data are displayed in Figure 7, and all relative rate coefficients that were obtained are summarized in Table 5. Data obtained with formaldehyde, acetaldehyde, and ethane as the reference compounds in either air or N_2 diluent, and at total pressures of either 30 or 720 Torr, all provide consistent values for k_4, which fall in the range (2.3−2.7) × 10^{-11} cm^3 molecule^{-1} s^{-1}. Data obtained in air with methanol as the reference compound also provided a k_4 value consistent with these data, $k_4 = 2.2 \times 10^{-11}$ cm^3 molecule^{-1} s^{-1}. However, inconsistent results were obtained in N_2 using methanol as the reference. Initial experiments, using the longer-wavelength photolysis lamp/filter combination (300−400 nm) yielded $k_4 = 1.8 \times 10^{-11}$ cm^3 molecule^{-1} s^{-1}, while later experiments with the UV-enhanced photolysis lamp yielded a higher value of 2.5×10^{-11} cm^3 molecule^{-1} s^{-1}. This methanol-related discrepancy was far more severe in the measurements of the Cl atom reaction with

TABLE 5: Summary of Relative Rate Coefficient (k_4) Determinations for Reaction of Cl Atom with Iodoethane[a]

reference compound	buffer gas (pressure)	rate coefficient ratio k_4/k_{ref}	reference reaction rate coefficient[59,60] (10^{-12} cm^3 molecule^{-1} s^{-1})	measured value for k_4 (10^{-12} cm^3 molecule^{-1} s^{-1})
formaldehyde	N_2 (720 Torr)	0.32	73	23
formaldehyde	N_2 (30 Torr)	0.36	73	26
methanol	Air (720 Torr)	0.40	55	22
ethane	Air (720 Torr)	0.43	57	25
acetaldehyde	N_2 (720 Torr)	0.34	79	27
acetaldehyde	N_2 (30 Torr)	0.34	79	27

[a] For formaldehyde and methanol, uncertainties in measured rate coefficient ratios are ±6%, while uncertainties in values for k_4 are ±10%. For acetaldehyde and ethane, uncertainties of ±10% and ±15% apply for the ratios and k_4 values, respectively.

TABLE 6: Product Yields (in %) from Oxidation of Iodoethane[a]

initial [iodoethane]	CH_3CHO[b]	CH_3CHO[c]	CH_3CHO[d]	ethene[e]	ethene[c]	ethene[d]	2-chloroethane	sum[f]
3.5×10^{14}	43	21	24	21	21	33	8	76
6.9×10^{14}	39	23	26	23	25	30	16	81
14×10^{14}	35	21	22	21	24	27	21	80
28×10^{14}	29	18	20	19	22	26	29	80
56×10^{14}	28	15	20	20	23	25	40	91

[a] Absolute uncertainties in product yields are ±(4−6)%. [b] (1a) Lower limit from sum of acetaldehyde, acetyl chloride, CH_2O, CO, and peracetic acid yields. [c] (2) From initial slope of [product] vs Δ[iodoethane] plots. [d] (3) From fits of product yield data to eq N or N′; see text for details. [e] (1b) Lower limit from sum of ethene and chloroacetaldehyde yields. [f] (4) Sum of column 1, the average of columns 4, 5, and 6, and column 7.

2-iodopropane, k_6, discussed below. Reasons for this discrepancy are not resolved at this time, but may involve a loss of methanol via reaction (gas-phase or at the reactor surfaces) with impurities present in the chamber at the time of the early experiments. Thus, in reporting a final value for k_4, we ignore the value obtained using methanol in N_2 diluent and average the data in Table 5, which yields $k_4 = (2.5 \pm 0.4) \times 10^{-11}$ cm^3 molecule^{-1} s^{-1}.

The value for k_4 obtained via the relative rate technique is significantly higher than that obtained by extrapolation of the high-temperature flash photolysis data to 298 K ($k_{4,abstraction} = 1.6 \times 10^{-11}$ cm^3 molecule^{-1} s^{-1}, see section 1.A above), or the value reported by Cotter et al.[23] in their low-pressure discharge-flow study, also $k_4 = 1.6 \times 10^{-11}$ cm^3 molecule^{-1} s^{-1}. The most likely explanation for these observations is that in the higher-concentration environment present for the relative rate determinations, loss of iodoethane is occurring not only via abstraction but also via formation and subsequent *irreversible* loss of the adduct in the chamber,[28] represented by reaction 22

$$Cl + CH_3CH_2I \leftrightarrow CH_3CH_2I{\cdot}Cl \quad (4c)$$

$$CH_3CH_2I{\cdot}Cl \rightarrow \text{products} \quad (22)$$

To quantitatively explain the observations, irreversible loss of iodoethane via adduct formation must contribute about 9×10^{-12} cm^3 molecule^{-1} s^{-1} to the observed rate coefficient, or about 10% of the value of the rate coefficient for adduct formation measured in the flash photolysis experiments. With adduct decomposition determined to be about 10^4 s^{-1} at 298 K in the flash photolysis experiments, irreversible adduct loss must then occur with a first-order rate coefficient of roughly 10^3 s^{-1}. Further discussion of the chemistry of the $CH_3CH_2I{\cdot}Cl$ adduct is presented in the following two sections.

F. Iodoethane Products. To determine the products of the Cl atom initiated oxidation of iodoethane, mixtures of Cl_2, (25−50) $\times 10^{14}$ molecule cm^{-3}, and iodoethane were photolyzed in the NCAR environmental chamber in the presence of 720 ± 20 Torr synthetic air. The initial iodoethane concentration, $[CH_3CH_2I]_0$, was varied over a wide range, (3.2−51) $\times 10^{14}$ molecule cm^{-3}. In all cases, products observed following photolysis were chloroethane, acetaldehyde, ethene, peracetic acid, chloroacetaldehyde, CO_2, acetyl chloride, formaldehyde, and CO. Product concentrations versus iodoethane consumption (for $[CH_3CH_2I]_0 = 14 \times 10^{14}$ molecule cm^{-3}) are presented in Figure 8a,b. On a per-carbon basis, the identified products accounted on average for 80 ± 12% of the reacted iodoethane. The major primary products are found to be acetaldehyde, ethene, and chloroethane; yield data for these three products, obtained over a range of $[iodoethane]_0$, are summarized in Table 6 and are discussed in detail below. The downward curvature observed in the yield plots for acetaldehyde and ethene indicates that these species are being consumed over the course of a run, a fact that is consistent with their rapid reaction with Cl atoms. Note that the reactions of Cl with ethene and acetaldehyde are about 4 and 3 times faster,[59] respectively, than the reaction of Cl with iodoethane. Upward curvature in the yield plots for peracetic acid, chloroacetaldehyde, and CO_2 indicates that these species arise from secondary sources. The small amounts of formaldehyde, acetyl chloride, and CO (not shown in Figure 8, but similar in magnitude to CH_2O) that are observed also likely arise from secondary chemistry, as is discussed in more detail below.

Three channels are expected to be operative in the reaction of Cl atoms with iodoethane, two abstraction channels and an adduct-forming channel

$$Cl + CH_3CH_2I \rightarrow CH_3CHI + HCl \quad (4a)$$

$$Cl + CH_3CH_2I \rightarrow CH_2CH_2I + HCl \quad (4b)$$

$$Cl + CH_3CH_2I \leftrightarrow CH_3CH_2I{\cdot}Cl \quad (4c)$$

Note that in the chamber system, these abstraction channels may,

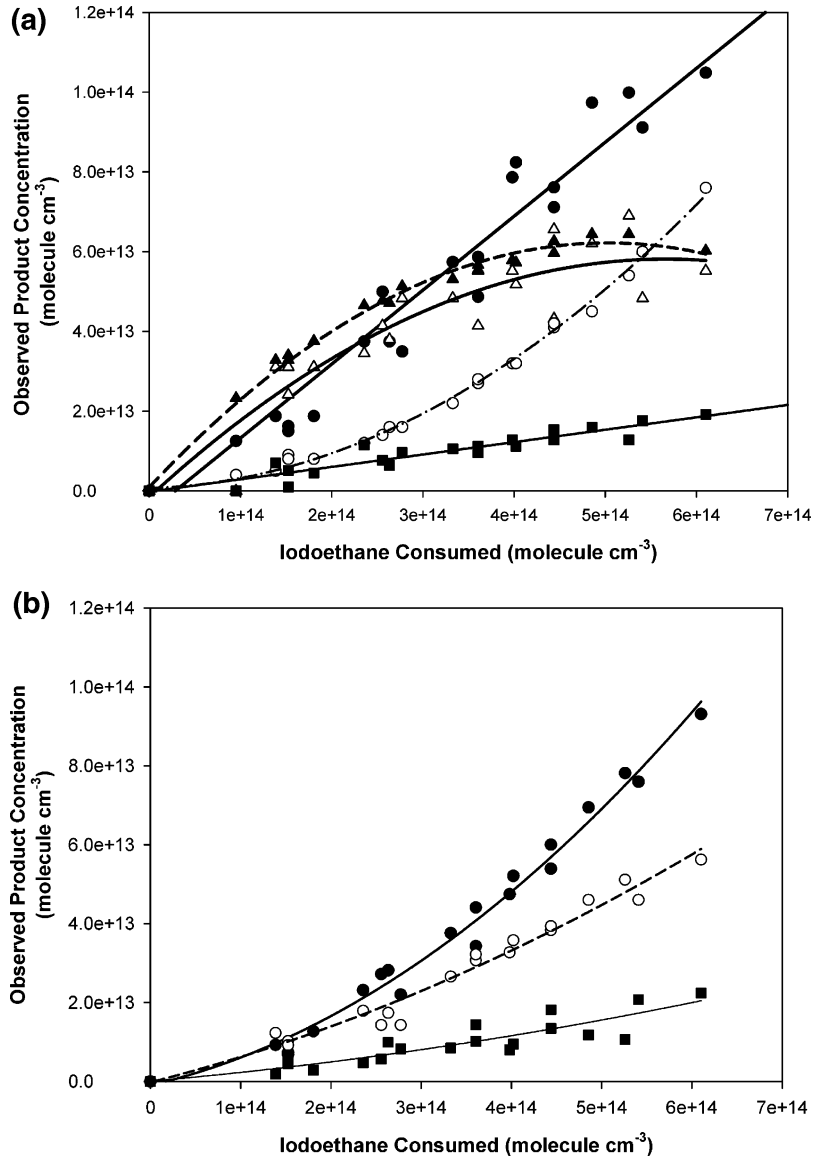

Figure 8. (a) Products observed in the Cl atom initiated oxidation of iodoethane, for $[CH_3CH_2I]_0 = 14 \times 10^{14}$ molecule cm^{-3} in 720 Torr air diluent: chloroethane, solid circles and solid line; ethene, solid triangles and dashed line; acetaldehyde, open triangles and solid curve; CO_2, open circles and dash−dot curve; formaldehyde, solid squares and solid line. (b) Products observed in the Cl atom initiated oxidation of iodoethane, for $[CH_3CH_2I]_0 = 14 \times 10^{14}$ molecule cm^{-3} in 720 Torr air diluent: peracetic acid, solid circles and solid curve (upper); chloroacetaldehyde, open circles and dashed curve; acetyl chloride, solid squares and solid curve (lower).

at least in part, involve the participation of the adduct, for example

$$Cl + CH_3CH_2I \rightarrow CH_3CH_2I{\cdot}Cl \rightarrow CH_3CHI + HCl \quad (4a)$$

As first described by Cotter et al.[24] and by analogy to the widely accepted chemistry of other alkyl radicals, pathway 4a is expected to lead to acetaldehyde, via the formation of 1-iodoethylperoxy radicals, reactions 7−9. Acetyl iodide, CH_3COI, might also be generated via self-reaction of the 1-iodoethylperoxy radicals or via their reaction with other peroxy radicals present in the system.

$$CH_3CHI + O_2 \rightarrow CH_3CHIOO^{\bullet} \quad (7)$$

$$2CH_3CHIOO^{\bullet} \rightarrow 2CH_3CHIO^{\bullet} + O_2 \quad (8a)$$

$$\rightarrow CH_3COI + CH_3CHIOH + O_2 \quad (8b)$$

$$CH_3CHIO^{\bullet} \rightarrow CH_3CHO + I \quad (9)$$

However, during the course of this work, Enami et al.[61] reported on the observation of IO from the reaction of CH_2I radicals with O_2, opening up the possibility of an alternative route to acetaldehyde production in the oxidation of 1-iodoethyl radicals

$$CH_3CHI + O_2 \rightarrow CH_3CHO + IO^{\bullet} \quad (23)$$

Regardless of the actual mechanism for acetaldehyde production, its subsequent oxidation would likely lead to the formation of trace amounts of acetyl chloride via reaction 25, as well as CO_2, CH_2O, CO, acetic acid, peracetic acid, and CH_3OH from the well-established[59,62,63] chemistry of the peroxyacetyl radical product of reaction 26

$$Cl + CH_3CHO \rightarrow CH_3CO + HCl \quad (24)$$

$$CH_3CO + Cl_2 \rightarrow CH_3COCl + Cl \quad (25)$$

$$CH_3CO + O_2 + M \rightarrow CH_3C(O)O_2 + M \quad (26)$$

Despite this rapid secondary chemistry, a variety of independent

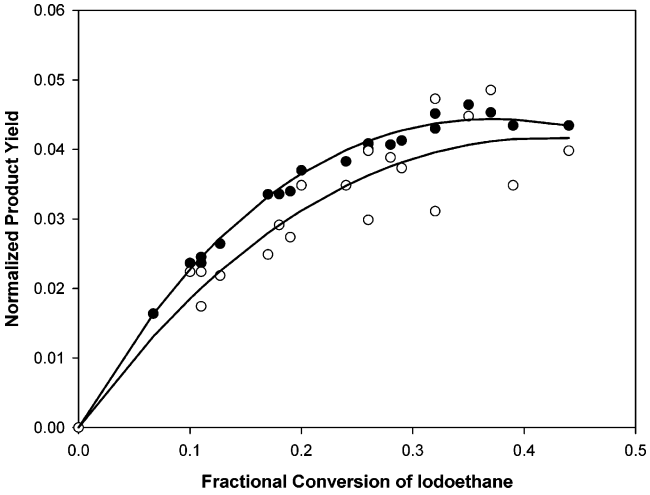

Figure 9. Normalized product yields vs fractional iodoethane conversion, $[CH_3CH_2I]_0 = 14 \times 10^{14}$ molecule cm^{-3}, 720 Torr air diluent: ethene, solid circles and upper line; acetaldehyde, open circles and lower line.

means are available with which to assess the initial CH_3CHO yield, and hence to estimate the branching into reaction 4a. One method is from the examination of the initial slopes of plots of $\Delta[CH_3CHO]$ vs $-\Delta[CH_3CH_2I]$ (i.e., from a determination of the linear term in quadratic fits to the data). Acetaldehyde yields estimated in this manner over a range of $[CH_3CH_2I]_0$ are shown in Table 6 and vary from 15% to 23% with a slight decreasing trend in the yield with increasing $[CH_3CH_2I]_0$.

Another method of obtaining the initial CH_3CHO yield is from an analysis of the kinetic mechanism (reactions 4a, 7−9 or 23, and 24), which yields the following expression for the CH_3CHO temporal profile[64]

$$f_{CH_3CHO} = Y_{CH_3CHO}\cdot(1 - f_{CH_3CH_2I})\cdot[(1 - f_{CH_3CH_2I})^{(k_{24}/k_4 - 1)} - 1]/(1 - k_{24}/k_4) \quad \text{(N)}$$

Here, f_{CH_3CHO} refers to the concentration of CH_3CHO, normalized to $[CH_3CH_2I]_0$, Y is the fractional yield of CH_3CHO per iodoethane oxidized, and $f_{CH_3CH_2I}$ is the fraction of the initial iodoethane that has been oxidized.[64] Thus, values for the CH_3CHO yield (Y) could be obtained from least-squares fits of eq N to plots of f_{CH_3CHO} vs $f_{CH_3CH_2I}$ data. Fitting was done first on the individual data sets obtained at each $[\text{iodoethane}]_0$ and then on the entire data set. The rate coefficient ratio k_{24}/k_4 was fixed at a value of 3.0, derived from a combination of the relative rate determination of k_4 described above and the literature value for k_{24},[59] and only the value of Y was treated as a fit parameter. Data obtained from these fits are summarized in Table 6, and the fit to the data set obtained at $[CH_3CH_2I]_0 = 14 \times 10^{14}$ molecule cm^{-3} is shown in Figure 9 as an example. Retrieved values for Y_{CH_3CHO} varied between 0.19 and 0.26 for the individual data sets, with a decreasing trend in Y_{CH_3CHO} as a function of $[CH_3CH_2I]_0$. When the entire data set was employed, the retrieved value for Y_{CH_3CHO} was 0.26. Test fits conducted with k_{24}/k_4 and Y_{CH_3CHO} both treated as fit parameters generated consistent results, with retrieved values for k_{24}/k_4 varying between 2.7 and 3.5 and Y_{CH_3CHO} data essentially unchanged from fits obtained with k_{24}/k_4 fixed. Thus, the yield data obtained from fits to eq N are consistent with those derived from the initial slope analysis and suggest a yield for acetaldehyde near 20% with a slight negative correlation with $[CH_3CH_2I]_0$ in evidence.

An estimate of the acetaldehyde yield can also be made from a consideration of the chemistry that can occur following reaction 24.[59,62,63] The oxidation of acetaldehyde can result in the formation of the following carbon-containing end products: CH_3COCl, peracetic acid, acetic acid, and CO_2 with either CH_2O, CH_3OH, CH_3OOH, or CO as a coproduct. Because other sources exist for CO_2 (e.g., from the oxidation of chloroacetaldehyde, itself a byproduct of ethene) and because CH_3OH, acetic acid, and CH_3OOH were not observed, it was thought that plots of the sum of the CH_3CHO, CH_3COCl, peracetic acid, CH_2O, and CO concentrations against the loss of CH_3CH_2I could provide another means for estimating the CH_3CHO yield. Technically, this should yield a lower limit to the actual yield, since CH_3OH, CH_3OOH, and acetic acid may have been present, but at levels below the detection limit. CH_3CHO yields obtained from this summation procedure, as summarized in Table 6, range from 0.28 to 0.43 with a clear anti-correlation with $[CH_3CH_2I]_0$.

Interestingly, acetaldehyde yields obtained from this analysis of the products generated via secondary chemistry (28−43%) are higher than those derived from an analysis of the acetaldehyde concentration data alone (about 20%). Thus, box-model simulations of the iodoethane oxidation process were run using the Acuchem software package[65] to explore this apparent discrepancy (i.e., to examine consistency between the measured and modeled product concentration data). Accurate modeling was difficult because of the occurrence of self- and cross-reactions involving the various peroxy radicals likely formed (CH_3CHIO_2, $ClCH_2CH_2O_2$, CH_3COO_2, CH_3O_2, HO_2, etc.), for which rate coefficient and product branching ratio information is limited. However, when estimates were made for the rates of these processes using the observations to constrain the model to the best extent possible, it was apparent that measured peracetic acid levels were much higher (about an order of magnitude) than could be explained by the model. Thus, it is concluded that there is a peracetic acid source other than the only modeled source, the reaction of $CH_3C(O)O_2$ with HO_2[59,63]

$$CH_3C(O)O_2 + HO_2 \rightarrow CH_3C(O)OOH + O_2 \quad \text{(27a)}$$

$$CH_3C(O)O_2 + HO_2 \rightarrow CH_3C(O)OH + O_3 \quad \text{(27b)}$$

$$CH_3C(O)O_2 + HO_2 \rightarrow CH_3C(O)O + OH + O_2 \quad \text{(27c)}$$

Additional evidence for another peracetic acid source comes from the fact that no acetic acid is observed in the product spectra, even though it would be easily detectible at the levels expected if reaction 27 was the major source of the observed peracetic acid. An intriguing possibility for the missing source of peracetic acid is via acetyl iodide, CH_3COI, possibly formed via reaction 8b or via analogous pathways in the reactions of CH_3CHIO_2 (if formed) with other peroxy radicals. Box-model results indicate that production of acetyl iodide may be important, even for branching ratios to molecular channels such as reaction 8b as low as 10% or so. Conversion of acetyl iodide to peracetic acid could possibly occur via the reaction of HO_2 with CH_3COI

$$CH_3C(O)I + HO_2 \rightarrow CH_3C(O)OOH + I \quad \text{(28)}$$

HO_2 is known to add reversibly to carbonyl compounds,[66,67] and it is at least possible that the existence of an exothermic I atom elimination channel pushes this reaction through to peracetic acid and I atom products. However, iodoethane oxidation experiments conducted in the presence of elevated HO_2 levels (generated via addition of either CH_2O or CH_3OH

to standard Cl_2/iodoethane/air mixtures) did not reveal any increase in the yield of peracetic acid, thus eliminating reaction 28 as the missing peracetic acid source.

Regardless of the details of the actual peracetic acid source chemistry, it is almost certain that it originates from chemistry occurring following abstraction from the $-CH_2I$ group in iodoethane. Thus, the analysis based on CH_3CHO, CH_3COCl, peracetic acid, CH_2O, and CO product yields presented above likely provides the best estimate of branching ratios to reaction 4a. It can then be concluded that this reaction channel accounts for about 28−43% of the reaction at atmospheric pressure, with a definite trend to lower yields with increasing $[CH_3CH_2I]_0$. True branching to reaction channel 4a could be slightly higher, since certain hydroperoxides (e.g., $CH_3CHIOOH$) may be formed, but may not be detectible and/or may decompose on our chamber surfaces.

Ethene is clearly observed as a primary product of the Cl atom initiated oxidation of iodoethane; see Figure 8 for representative data. As described in the Introduction, ethene is a possible product following H atom abstraction from the CH_3 group in iodoethane

$$Cl + CH_3CH_2I \rightarrow CH_2CH_2I + HCl \qquad (4b)$$

$$CH_2CH_2I \rightarrow CH_2{=}CH_2 + I \qquad (13)$$

The observed decrease in the apparent C_2H_4 yield with increasing consumption of CH_3CH_2I is consistent with its rapid reaction with Cl atoms; $k_{29} = 1.0 \times 10^{-10}$ cm^3 molecule^{-1} s^{-1} [59]

$$Cl + CH_2CH_2 + M\ (+O_2) \rightarrow ClCH_2CH_2O_2 + M \qquad (29)$$

Thus, to determine the initial ethene yield, the same procedures were used as were just outlined for the CH_3CHO yield determinations. Data obtained by the three independent methods are summarized in Table 6. First, determination of the initial slopes of plots of $[C_2H_4]$ vs $-\Delta[CH_3CH_2I]$ led to the derivation of initial C_2H_4 yields of about 23%, independent of the initial $[CH_3CH_2I]$. Second, the observed fractional yields of C_2H_4 versus fractional CH_3CH_2I consumption were fit to an equation analogous to eq N.[64]

$$f_{C_2H_4} = Y\cdot(1 - f_{CH_3CH_2I})\cdot[(1 - f_{CH_3CH_2I})^{(k_{29}/k_4 - 1)} - 1]/(1 - k_{29}/k_4) \qquad (N')$$

Here, $f_{C_2H_4}$ refers to the concentration of C_2H_4, normalized to $[CH_3CH_2I]_0$, Y is the fractional yield of C_2H_4 per iodoethane oxidized, and $f_{CH_3CH_2I}$ is the fraction of the initial iodoethane that has been oxidized. The rate coefficient ratio k_{29}/k_4 was fixed to a value of 4.0 ($k_4 = 2.5 \times 10^{-11}$ cm^3 molecule^{-1} s^{-1}, this work; $k_{29} = 1.0 \times 10^{-10}$ cm^3 molecule^{-1} s^{-1}),[59] and fits were conducted on the individual data sets obtained at each $[CH_3CH_2I]_0$. Initial C_2H_4 yields obtained via this method ranged from 0.25 to 0.33 and displayed a slight anti-correlation with $[CH_3CH_2I]_0$.

Since chloroacetaldehyde, $ClCH_2CHO$, is the major product of the Cl atom initiated oxidation of ethene

$$ClCH_2CH_2O_2 + RO_2 \rightarrow ClCH_2CH_2O + RO + O_2 \qquad (30)$$

$$ClCH_2CH_2O + O_2 \rightarrow ClCH_2CHO + HO_2 \qquad (31)$$

plots of observed $\{[ClCH_2CHO] + [C_2H_4]\}$ vs $-\Delta[CH_3CH_2I]$ also provide a means for estimating the initial C_2H_4 yield. This procedure led to C_2H_4 yields ranging from 19% to 23%. Note that, since chloroacetaldehyde is not the sole product of ethene consumption and it too is reactive with Cl atoms, this method should technically be considered an upper limit. Nonetheless, the three methods of data analysis are in rough accord and indicate a C_2H_4 yield of about 20−30%.

Last, we note that the yield of ethene did not vary with O_2 partial pressure (20−500 Torr), indicating that addition of O_2 to CH_2CH_2I is not likely competing with decomposition via reaction 13. Thus, C_2H_4 is likely the predominant product resulting from abstraction at the methyl group in iodoethane, and the measured C_2H_4 yields should provide a reasonable measure of the branching ratio to reaction 4b.

The third major primary product of the Cl atom initiated oxidation of iodoethane was chloroethane; see Figure 8 for representative product yield data. Since the reaction of chloroethane with Cl atoms is relatively slow, 8×10^{-12} cm^3 molecule^{-1} s^{-1},[68] secondary loss of this species was minimal. Yield data, corrected for this secondary loss using a rearranged version of eq N,[64] are presented in Table 6 and show a strong correlation with $[CH_3CH_2I]_0$, increasing from about 0.08 to 0.40 as $[CH_3CH_2I]_0$ was varied from $(3.5-56) \times 10^{14}$ molecule cm^{-3}. The observation of increasing chloroalkane yield with increasing $[\text{iodoalkane}]_0$ is in keeping with what was noted by Bilde and Wallington[28] in their study of the Cl atom initiated oxidation of CH_3I. These authors reported yields of CH_3Cl that increased from ~15% at $[CH_3I]_0 = 1.6 \times 10^{14}$ molecule cm^{-3} to as high as 80% at $[CH_3I]_0 = 250 \times 10^{14}$ molecule cm^{-3}. In addition, they observed a noticeable increase in the effective rate coefficient for reaction of Cl with CH_3I (as measured by the relative rate technique) as the initial $[CH_3I]$ increased. They rationalized these observations in terms of a reaction of the Cl/CH_3I adduct with a second CH_3I molecule, a process that leads to the production of CH_3Cl and competes with adduct decomposition, reaction (−1b)

$$Cl + CH_3I \leftrightarrow CH_3I\cdot Cl \qquad (1b)$$

$$CH_3I\cdot Cl \rightarrow \text{products} \qquad (2)$$

$$CH_3I + CH_3I\cdot Cl \rightarrow CH_3Cl + \text{other products (likely } CH_3I \text{ and I)} \qquad (3)$$

Our data then suggest the occurrence of a similar mechanism, leading to the formation of chloroethane with a yield that is correlated with $[CH_3CH_2I]_0$

$$Cl + CH_3CH_2I \leftrightarrow CH_3CH_2I\cdot Cl \qquad (4c)$$

$$CH_3CH_2I\cdot Cl \rightarrow \text{products} \qquad (23)$$

$$CH_3CH_2I + CH_3CH_2I\cdot Cl \rightarrow CH_3CH_2Cl + CH_3CH_2I + I \qquad (32)$$

The possibility of the occurrence of a bimolecular halogen exchange reaction 4d

$$Cl + CH_3CH_2I \rightarrow CH_3CH_2Cl + I \qquad (4d)$$

cannot be ruled out, although this pathway can account for no more than about 10% of the overall reaction, $k_{4d} < 2.5 \times 10^{-12}$ cm^3 molecule^{-1} s^{-1}.

In contrast to the observations of Bilde and Wallington, however, an increase in the effective rate coefficient for reaction 4 with increasing $[CH_3CH_2I]_0$, $(2.5-25) \times 10^{14}$ molecule cm^{-3}, was not observed in the present work. This apparent discrepancy may be due to differences in experimental conditions in the two

cases, as well as to the existence of subtle differences in the chemistry of the adducts involved. First, the highest iodoethane concentrations employed in our relative rate experiments are an order of magnitude lower than those used by Bilde and Wallington, thus minimizing the effects of reaction 32 on the observed value of k_4. Second, for a given [iodoalkane]$_0$, less chloroalkane is observed in the iodoethane system than in the methyl iodide system; box modeling suggests a rate coefficient of $(5-10) \times 10^{-13}$ cm^3 molecule^{-1} s^{-1} for reaction 3, compared to only $(2-5) \times 10^{-13}$ cm^3 molecule^{-1} s^{-1} for reaction 32. Furthermore, in the case of the CH_3I/Cl adduct, first-order adduct loss via processes that do not regenerate Cl atoms, reaction 2, occurs at about 200 s^{-1}.[27,28] In the case of the Cl/CH_3CH_2I adduct, however, first-order loss of the adduct in the chamber system, reaction 22, was estimated in section 1.E to occur at a rate of about 10^3 s^{-1}. Thus, for $[CH_3CH_2I] \leq 25 \times 10^{14}$ molecule cm^{-3} as employed in our relative rate studies of reaction 4, the first-order rate of occurrence of reaction 32 is probably less than the competing loss channels for the adduct. Thus, a large increase in the observed value for k_4 is not expected. In fact, simulations suggest that a change in k_4 of only about ±10% would be expected over the range of $[CH_3CH_2I]_0$ employed in the relative rate experiments, just on the edge of what is likely to be detectible.

To summarize, the three channels identified in the reaction of Cl atoms with iodoethane, reactions 4a−c leading to the formation of acetaldehyde, ethene, and chloroethane, respectively, account for about 80−85% of the reacted iodoethane (see summary given in Table 6). The reaction channel most likely to be underestimated is reaction 4a, given the possibility of the formation of unquantified products such as $CH_3CHIOOH$, CH_3COI, CH_3OH, acetic acid, and so on. The product yield data can be used to derive site-specific rate coefficients, $k_{4a} \geq 1 \times 10^{-11}$ cm^3 molecule^{-1} s^{-1} and $k_{4b} \approx 6 \times 10^{-12}$ cm^3 molecule^{-1} s^{-1}. These results can be combined with literature data[33,60,64,69-71] to examine reactivity trends along the series of monohalogenated ethanes. Abstraction at the $-CH_3$ group increases smoothly from roughly 7×10^{-13} cm^3 molecule^{-1} s^{-1} for CH_3CH_2F, 1.4×10^{-12} cm^3 molecule^{-1} s^{-1} for CH_3CH_2Cl, and 4×10^{-12} cm^3 molecule^{-1} s^{-1} for CH_3CH_2Br to about 6×10^{-12} cm^3 molecule^{-1} s^{-1} for CH_3CH_2I. A less pronounced trend for abstraction at the $-CH_2-X$ group is evident; k_{-CH_2-X} is about 7×10^{-12} cm^3 molecule^{-1} s^{-1} for CH_3CH_2F and CH_3CH_2Cl and about 1×10^{-11} cm^3 molecule^{-1} s^{-1} for both CH_3CH_2Br and CH_3CH_2I.

Last, we compare our product distributions with those reported by Cotter et al.[24] These authors report a chloroethane yield of 45% for an initial [iodoethane] $\approx 20 \times 10^{14}$ molecule cm^{-3}, a value that is higher than what is observed (≈25%) in the current study for similar conditions (see Table 6). Their value for the branching to reaction 4a, about 45%, is also somewhat higher than what we observe (although within mutual uncertainties). Cotter et al. do not report the formation of ethene in the Cl atom initiated oxidation of iodoethane, while in the present work, this species is clearly observed as a primary product (yield ≈ 25%). The low IR absorption cross-section for ethene, the overlap of its main absorption feature with a major iodoethane absorption feature, and its low steady-state levels due to secondary consumption may have contributed to this discrepancy.

The data presented in sections 1.A−1.F above can be combined to present a complete picture of the mechanism of the Cl atom/iodoethane reaction and subsequent chemistry occurring under atmospheric conditions. The following conclusions can be drawn:

(i) Extrapolation of the high-temperature flash photolysis results to 298 K suggests that pure abstraction pathways in the reaction of Cl atoms with iodoethane occur with a rate coefficient $(k_{4a} + k_{4b}) = 1.6 \times 10^{-11}$ cm^3 molecule^{-1} s^{-1}, in accord with Cotter et al.[23]

(ii) Reversible adduct formation and loss, reactions 4c and −4c, occur with rate coefficients of about 7×10^{-11} cm^3 molecule^{-1} s^{-1} and 1.1×10^4 s^{-1}, respectively, at 298 K and 300 Torr. Since the high-pressure limit for these reactions has not likely been reached, somewhat larger rate coefficients would apply at 1 atm total pressure.

(iii) The binding energy for the Cl atom/iodoethane adduct, as determined from the flash photolysis experiments and the theoretical studies, is approximately 60 kJ mol^{-1}.

(iv) Relative rate studies generate an effective value for $k_4 \approx 2.5 \times 10^{-11}$ cm^3 molecule^{-1} s^{-1} at 298 K, 1 atm pressure, larger than the extrapolated abstraction rate coefficient. This suggests the participation of the adduct in the removal of iodoethane in the environmental chamber experiments.

(v) Acetaldehyde and ethene are observed as primary products in the chamber experiments. These products are obtained from reactions 4a and 4b, respectively, which account for roughly 35% and 25% of the total reaction for $[CH_3CH_2I]_0 \approx 10^{15}$ molecule cm^{-3}.

(vi) A reaction between the Cl/iodoethane adduct and a second iodoethane molecule has been identified, $k_{32} \approx (2-5) \times 10^{-13}$ cm^3 molecule^{-1} s^{-1}, leading to the production of chloroethane with a yield that correlates with the initial iodoethane concentration.

2. Relative Rate and Product Studies for Reaction of Cl with 2-Iodopropane. *A. Relative Rate Measurements.* The rate coefficient for reaction of Cl atoms with 2-iodopropane, k_6, was determined at 298 K in the NCAR environmental chamber via the relative rate technique. Values for k_6 were determined relative to k_{33} (in air and N_2 diluent at 720 Torr total pressure), k_{18} (in 720 Torr air, 720 Torr N_2, and 40 Torr N_2 diluent), and k_{19} (in 720 Torr air, 720 Torr N_2, and 20 Torr N_2 diluent)

$$Cl + CH_3CH_2Cl \rightarrow \text{products} \quad (33)$$

$$Cl + CH_2O \rightarrow HCO + HCl \quad (18)$$

$$Cl + CH_3OH \rightarrow CH_2OH + HCl \quad (19)$$

For measurements versus k_{18} in air, small corrections (<10%) were made to the measured CH_2O decays to account for conversion of CH_2O to HCOOH via reaction with HO_2. All data are summarized in Table 7, while a subset of these data is plotted in Figure 10. As can be seen from the Table, values for k_6 obtained versus k_{33} and k_{18} in either air or N_2 buffer gas, at 720 Torr total pressure or at 40 Torr total pressure (N_2 only), and over a range of 2-iodopropane concentrations spanning an order of magnitude are all consistent and yield an average value for k_6 of $(5.0 \pm 0.7) \times 10^{-11}$ cm^3 molecule^{-1} s^{-1}. The value obtained for k_6 in air with methanol as the reference compound, 5.1×10^{-11} cm^3 molecule^{-1} s^{-1}, is consistent with these findings. However, as was the case for k_4, inconsistencies were observed when using methanol as the reference compound in N_2 diluent; values obtained initially (2.1×10^{-11} cm^3 molecule^{-1} s^{-1}) were more than a factor of 2 lower than the value obtained in a later set of experiments (5.1×10^{-11} cm^3 molecule^{-1} s^{-1}). As discussed above for the case of iodoethane, reasons for this discrepancy are not resolved at this time. The final reported

TABLE 7: Summary of Relative Rate Coefficient Determinations for Reaction of Cl Atom Reaction with 2-Iodopropane, k_6[a]

reference compound	buffer gas (pressure)	rate coefficient ratio k_6/k_{ref}	reference reaction rate coefficient[59,60,68] (10^{-12} cm^3 molecule^{-1} s^{-1})	measured value for k_6 (10^{-12} cm^3 molecule^{-1} s^{-1})
chloroethane	air (720 Torr)	5.9	8.3	49
chloroethane	N_2 (720 Torr)	5.9	8.3	49
formaldehyde	air (720 Torr)	0.68	73	50
formaldehyde	N_2 (40 Torr)	0.73	73	53
formaldehyde	N_2 (720 Torr)	0.67	73	49
methanol	air (720 Torr)	0.93	55	51

[a] Uncertainties in measured rate coefficient ratios are 5−7%, while uncertainties in derived values for k_6 are 10−12%.

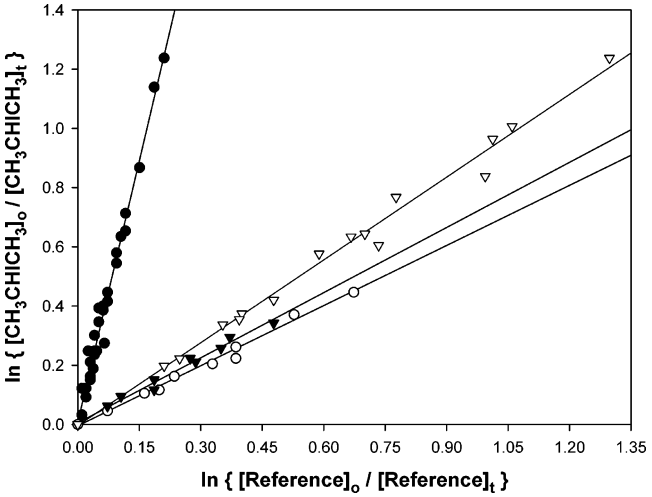

Figure 10. Relative rates of decay of CH_3CHICH_3 vs CH_3CH_2Cl (solid circles, 720 Torr air), vs CH_3OH (open triangles, 720 Torr air), vs CH_2O (solid triangles, 40 Torr N_2), and vs CH_2O (open circles, 720 Torr air) in the presence of Cl atoms.

value for k_6, which does not take into consideration the methanol data obtained in N_2, is $(5.0 \pm 0.7) \times 10^{-11}$ cm^3 molecule^{-1} s^{-1}, in very good agreement with the value previously reported by Cotter et al.[23] in a low-pressure, discharge flow tube system, $(4.68 \pm 0.49) \times 10^{-11}$ cm^3 molecule^{-1} s^{-1}. The similarity between the low- and high-pressure rate coefficients implies at most a modest contribution of adduct-related chemistry to the effective rate coefficient observed in our higher-pressure chamber studies.

B. 2-Iodopropane Products. To investigate the mechanism of the Cl atom initiated oxidation of 2-iodopropane, mixtures of Cl_2, $(25-50) \times 10^{14}$ molecule cm^{-3}, and 2-iodopropane, $(3.5-42) \times 10^{14}$ molecule cm^{-3}) were photolyzed in the environmental chamber in 720 ± 15 Torr air diluent. Products observed via IR absorption spectroscopy were acetone, 2-chloropropane, propene, and chloroacetone, which accounted on average for (85 ± 15)% of the 2-iodopropane consumed. Typical product yield data, for an initial [2-iodopropane] $= 14 \times 10^{14}$ molecule cm^{-3}, are shown in Figure 11.

Appearance profiles for acetone (i.e., plots of acetone production vs 2-iodopropane consumption; see Figure 11 for example) were linear, indicating that it is a primary product of the oxidation. Furthermore, since acetone reacts much more slowly with Cl atoms[59] than does 2-iodopropane (by a factor of about 25), no correction for secondary loss is necessary. Acetone yields can thus be obtained directly from the slopes of plots of [acetone] vs Δ[2-iodopropane]. Yields, obtained over a range of [2-iodopropane]$_0$ and shown in Table 8, varied from 26% to 33% and show a slight anti-correlation with [2-iodopropane]$_0$. As discussed by Cotter et al.,[24] acetone can be generated following H atom abstraction from the 2-position in 2-iodopropane (reaction 6a), followed by reactions 34−36

$$Cl + CH_3CHICH_3 \rightarrow CH_3C\cdot ICH_3 \quad (6a)$$

$$CH_3C\cdot ICH_3 + O_2 \rightarrow CH_3CI(OO^\bullet)CH_3 \quad (34a)$$

$$2CH_3CI(OO^\bullet)CH_3 \rightarrow 2CH_3CI(O^\bullet)CH_3 + O_2 \quad (35)$$

$$CH_3CI(O^\bullet)CH_3 \rightarrow CH_3C(=O)CH_3 + I \quad (36)$$

Again, there is a possibility of the involvement of a Cl/CH_3CHICH_3 adduct in the effective reaction 6a (and 6b; see below) in the high-pressure chamber experiments. Also, the recent experiments of Enami et al.,[61] referred to earlier, suggest the possibility of an alternate route to acetone production

$$CH_3C\cdot ICH_3 + O_2 \rightarrow CH_3C(=O)CH_3 + IO \quad (34b)$$

Propene is also observed as a primary product of the Cl atom initiated oxidation of 2-iodopropane, as illustrated in Figure 11. By analogy to ethene production from iodoethane, propene is the expected end product of abstraction from the methyl groups in 2-iodopropane

$$Cl + CH_3CHICH_3 \rightarrow CH_3CHICH_2^\bullet \quad (6b)$$

$$CH_3CHICH_2^\bullet \rightarrow CH_3CH{=}CH_2 + I \quad (37)$$

Because the propene appearance profiles (yields) did not vary with O_2 partial pressure (20−500 Torr), addition of O_2 to $CH_3CHICH_2^\bullet$ does not appear to compete with reaction 37. Propene reacts rapidly with Cl atoms; $k_{38} = 2.6 \times 10^{-10}$ cm^3 molecule^{-1} s^{-1} [59]

$$Cl + CH_2{=}CH{-}CH_3\ (+O_2) \rightarrow ClCH_2{-}CH(OO^\bullet){-}CH_3 \quad (38)$$

and so, a decrease in the apparent propene yield with 2-iodopropane consumption is observed. Thus, estimates of the true propene yield were obtained via the three methods used above for acetaldehyde and ethene data analysis.

Initial slopes of plots of Δ[propene] vs −Δ[2-iodopropane], as summarized in Table 8, indicated initial propene yields between 32% and 50%. A trend in the derived initial yields

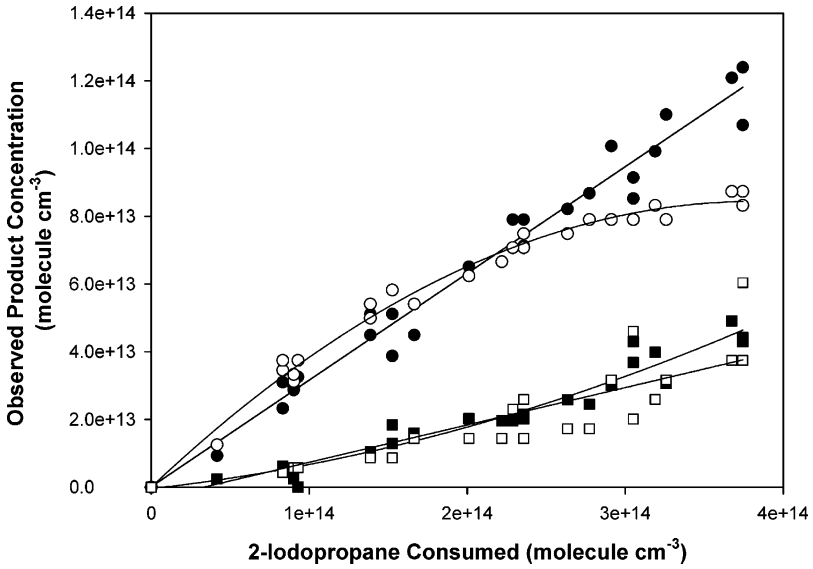

Figure 11. Products observed in the Cl atom initiated oxidation of 2-iodopropane, for $[CH_3CHICH_3]_0 = 14 \times 10^{14}$ molecule cm^{-3}, in 720 Torr air diluent: acetone, solid circles and solid line (upper); propene, open circles and solid curve (upper); 2-chloropropane, open squares and solid line (lower); chloroacetone, solid squares and solid line (lower).

TABLE 8: Product Yields (in %) from Oxidation of 2-Iodopropane[a]

[2-iodopropane]$_o$	acetone	propene[b]	propene[c]	propene[d] k_{33}/k_6 fixed	2-chloropropane
3.5×10^{14}	31	34	31	51	6
6.9×10^{14}	31	31	34	51	9
14×10^{14}	32	38	44	48	11
28×10^{14}	27	42	50	50	21
42×10^{14}	26	42	45	46	17
entire data set				50	

[a] Absolute uncertainties in product yields are ±6%, except for 2-chloropropane (±4%). [b] (1) Lower limit from sum of propene and chloroacetone yields. [c] (2) From initial slope of [propene] vs Δ[2-iodopropane] plots. [d] (3) From fits of product yield data to eq N″; see text for details.

with increasing [2-iodopropane]$_0$ is observed, but this is not believed to be significant. Note that very low (and thus difficult to quantify) steady-state levels of propene are observed in experiments with low initial [2-iodopropane], while uncertainties arise in the high [2-iodopropane] experiments from the low 2-iodopropane conversions observed.

Initial propene yields were also obtained from fits of the fractional propene yield versus the fractional 2-iodopropane consumption to eq N″ [64]

$$f_{C_3H_6} = Y\cdot(1 - f_{C_3H_7I})\cdot[(1 - f_{C_3H_7I})^{(k_{38}/k_6 - 1)} - 1)/(1 - k_{38}/k_6) \quad (N'')$$

Here, k_6 and k_{38} are the bimolecular rate coefficients for the consecutive reactions that form and destroy propene, Y is the yield of propene per molecule of 2-iodopropane oxidized, $f_{C_3H_6}$ is [propene]/$[CH_3CHICH_3]_0$, and $f_{C_3H_7I}$ is the fraction of the initial 2-iodopropane that has been consumed. Fits were performed with the ratio k_{38}/k_6 fixed to a value of 5.3, ($k_{38} = 2.6 \times 10^{-10}$ cm^3 molecule^{-1} s^{-1};[59] $k_6 = 4.9 \times 10^{-11}$ cm^3 molecule^{-1} s^{-1}, this work) on the individual data sets obtained at each [2-iodopropane]$_0$ and on the data set as a whole. As shown in Table 8, a very consistent set of propene yields were retrieved, ranging between 0.46 and 0.51 for the individual data sets, with a propene yield of 0.50 obtained from the fit that included the entire data set.

Chloroacetone is expected to be the major (but not exclusive) product of propene oxidation.

$$2ClCH_2CH(OO^\bullet)CH_3 \rightarrow 2ClCH_2CH(O^\bullet)CH_3 + O_2 \quad (39a)$$

$$2ClCH_2CH(OO^\bullet)CH_3 \rightarrow ClCH_2CH(OH)CH_3 + ClCH_2C(=O)CH_3 + O_2 \quad (39b)$$

$$ClCH_2CH(O^\bullet)CH_3 + O_2 \rightarrow ClCH_2C(=O)CH_3 + HO_2 \quad (40)$$

Thus, the sum of the propene and chloroacetone yields can be considered as a lower limit to the branching to reaction 6b. This sum varied from about 32% to 42% over the range of [2-iodopropane]$_0$ studied; see Table 8.

Appearance profiles for 2-chloropropane were linear, indicating that it too is a primary oxidation product. The data in Figure 11 show that the yield of 2-chloropropane, for [2-iodopropane]$_0$ $= 14 \times 10^{14}$ molecule cm^{-3}, is (11 ± 4)%. As shown in Table 8, a significant correlation between the 2-chloropropane yield and [2-iodopropane]$_0$ was observed, with the yield of 2-chloropropane increasing from about 6% at the lowest [2-iodopropane]$_0$ to about 20% at the highest [2-iodopropane]$_0$ used. Again, this observation supports the supposition of Bilde and Wallington[28] that the production of chloroalkanes from the corresponding iodoalkane occurs via the formation of a Cl/iodoalkane adduct that undergoes subsequent reaction with another iodoalkane molecule

$$Cl + CH_3CHICH_3 \leftrightarrow (CH_3CHICH_3)\cdot Cl \quad (6c)$$

$$CH_3CHICH_3 + (CH_3CHICH_3)\cdot Cl \rightarrow CH_3CHClCH_3 + CH_3CHICH_3 + I \quad (41)$$

Formation of 2-chloropropane via a bimolecular reaction 6d can account for no more than about 6% of the overall reaction, $k_{6d} \leq 3 \times 10^{-12}$ cm^3 molecule^{-1} s^{-1}

$$Cl + CH_3CHICH_3 \rightarrow (CH_3CHClCH_3) + I \quad (6d)$$

On the basis of the product yields just described, the mechanism for the reaction of Cl atoms with 2-iodopropane under chamber

conditions can be summarized as follows. Formation of propene is likely the predominant primary product arising from reaction 6b, and thus, this pathway accounts for about 40−50% of the total reaction. The yield of acetone, about 30%, can be thought of as a strict lower limit to the branching to reaction 6a because of the possible formation of other products via reaction with peroxy radicals generated in the oxidation of propene, for example

$$CH_3CI(OO^\bullet)CH_3 + HO_2 \rightarrow CH_3CI(OOH)CH_3 + O_2 \quad (42)$$

$$CH_3CI(OO^\bullet)CH_3 + ClCH_2CH(OO^\bullet)CH_3 \rightarrow CH_3CI(OH)CH_3 + ClCH_2C(=O)CH_3 + O_2 \quad (43a)$$

$$\rightarrow \text{other products} \quad (43b)$$

Nonetheless, given the nearly 50% yield of propene and the observation of 2-chloropropane as a primary product as well, the fraction of the Cl atom attack occurring via reaction 6a is unlikely to exceed 40% or so. The remainder of the reaction, about 5−20% under the conditions studied, involves a complex mechanism leading to the formation of 2-chloropropane, that occurs via the formation of a Cl/2-iodopropane adduct.

As was the case for iodoethane, the product data derived here are different from those reported by Cotter et al.[24] These workers reported an acetone yield of (59 ± 11)%, measurably higher than our value. Their yield of 2-chloropropane, (34 ± 12)% for an initial 2-iodopropane concentration of about 10^{15} molecule cm^{-3}, is also somewhat higher than our yield under these conditions. Finally, propene, a major product in our work and one expected on the basis of our previous work with ethyl bromide oxidation, was not reported by Cotter et al.[24] Like ethene, this species has a relatively weak absorption cross-section and is lost quite rapidly via secondary reaction.

Because time-resolved studies have not been conducted for the Cl/2-iodopropane reaction, a detailed analysis of the reaction mechanism cannot be presented. Nonetheless, a few conclusions can be drawn:

(i) Acetone and propene are major primary products of the reaction of Cl with 2-iodopropane. These products arise from reactions 6a and 6b, respectively. Effective rate coefficients under environmental chamber conditions are about 2.0×10^{-11} cm^3 $molecule^{-1}$ s^{-1} for k_{6a} and about 2.5×10^{-11} cm^3 $molecule^{-1}$ s^{-1} for k_{6b}.

(ii) 2-Chloropropane is clearly a product of the chemistry. The fact that its yield is correlated with $[CH_3CHICH_3]_0$ indicates that it arises predominantly from a reaction between a Cl/CH_3-$CHICH_3$ adduct and another CH_3CHICH_3 and provides indirect evidence for the existence of an adduct.

(iii) A direct bimolecular halogen-exchange process to produce 2-chloropropane, if operative, can occur with a rate coefficient of no more than 3×10^{-12} cm^3 $molecule^{-1}$ s^{-1}.

(iv) The fact that there is little, if any, change in the value for k_6 between a few Torr[23] and 1 atm (this work) implies that the chemistry of the Cl/2-iodopropane adduct is dominated by decomposition to reactants, reaction (−6c), for typical chamber conditions.

3. Atmospheric Implications. The data obtained herein contribute to our overall understanding[19−24] of the atmospheric fate of iodoethane and 2-iodopropane, as well as the iodoalkanes in general. Clearly, photolysis represents a major sink for these compounds; for example, Cotter et al.[22] have estimated globally and diurnally averaged lifetimes of 4 and 2 days for iodoethane and 2-iodopropane, respectively, using literature cross-section data.[18,19] Reaction with OH[21,22] will also play a role in the destruction of these species; with a globally averaged [OH] = 10^6 molecule cm^{-3}, lifetimes of 17 and 8 days can be estimated for these two species. The estimation of lifetimes with respect to Cl atom reaction is more difficult given the uncertainty in, and likely spatial and temporal variability of, Cl atom concentrations and the unknown atmospheric fate of the Cl/iodoalkane adducts. Assuming [Cl] = 10^4 molecule cm^{-3} in the MBL[25] and that no iodoalkane loss results from adduct formation, lifetimes of 70 and 23 days are derived for iodoethane and 2-iodopropane. Under the assumption of efficient iodoalkane destruction upon formation of an adduct with Cl, the iodoethane lifetime would be reduced to about 17 days, and a similar 2-iodopropane lifetime is likely. Finally, as noted by Cotter et al.,[22] should higher [Cl] = 10^5 molecule cm^{-3} apply in some cases,[26] reaction with Cl could become a very efficient sink for these species, comparable to removal by photolysis.

Acknowledgment. The National Center for Atmospheric Research (NCAR) is operated by the University Corporation for Atmospheric Research, under the sponsorship of the National Science Foundation. Thanks are due to David Hanson and Chris Cantrell of NCAR for their comments on the manuscript. The research at NCAR was funded in part by the NASA Upper Atmosphere Research Program. The research at Georgia Tech was funded in part by the NASA Upper Atmosphere Research Program and in part by the NSF Atmospheric Chemistry Program. Computer time for this study was made available by the Alabama Supercomputer Network.

References and Notes

(1) Chameides, W. L; Davis, D. D. *J. Geophys. Res.* **1980**, *85*, 7383.
(2) Cicerone, R. J. *Rev. Geophys. Space Phys.* **1981**, *190*, 123.
(3) Vogt, R. Iodine compounds in the atmosphere. In *The Handbook of Environmental Chemistry Volume 4E, Reactive Halogen Compounds in the Atmosphere*; Fabian, P., Singh, O. N., Eds.; Springer-Verlag: Heidelberg, 1999.
(4) Lovelock, J. E.; Maggs, R. J.; Wade, R. J. *Nature (London)* **1973**, *241*, 194.
(5) Atlas, E.; Pollock, W.; Greenberg, J.; Heidt, L.; Thompson, A. M. *J. Geophys. Res.* **1993**, *98*, 16933.
(6) Carpenter, L. J.; Sturges, W. T.; Penkett, S. A.; Liss, P. S.; Alicke, B.; Hebestreit, K.; Platt, U. *J. Geophys. Res.* **1999**, *104*, 1679.
(7) Davis, D.; Crawford, J.; Liu, S.; McKeen, S.; Bandy, A.; Thornton, D.; Rowland, F.; Blake, D. *J. Geophys. Res.* **1996**, *101*, 2135.
(8) Moore, R. M.; Groszko, W. *J. Geophys. Res.* **1999**, *104*, 11163.
(9) Yokouchi, Y.; Mukai, H.; Yamamoto, H.; Otsuk, A.; Saitoh, C.; Nojiri, Y. *J. Geophys. Res.* **1997**, *102*, 8805.
(10) Yokouchi, Y.; Nojiri, Y.; Barrie, L. A.; Toom-Sauntry, D.; Fujinuma, Y. *J. Geophys. Res.* **2001**, *106*, 12661.
(11) Klick, S.; Abrahamsson, K. *J. Geophys. Res.* **1992**, *97*, 12683.
(12) Moore, R. M.; Tokarczyk, R. *Geophys. Res. Lett.* **1992**, *19*, 1779.
(13) Jimenez, J. L.; Bahreini, R.; Cocker, D. R., III; Zhuang, H.; Varutbangkul, V.; Flagan, R. C.; Seinfeld, J. H.; O'Dowd, C. D.; Hoffmann, T. *J. Geophys. Res.* **2003**, *108*, 4308; doi: 10.1029/2002JD002452.
(14) Burkholder, J.; Curtius, J.; Ravishankara, A. R.; Lovejoy, E. *Atmos. Chem. Phys.* **2004**, *4*, 19.
(15) McFiggans, G.; Coe, H.; Burgess, R.; Allan, J.; Cubison, M.; Rami Alfarra, M.; Saunders, R.; Saiz-Lopez, A.; Plane, J.; Wevill, D.; Carpenter, L.; Rickard, A.; Monks, P. *Atmos. Chem. Phys.* **2004**, *4*, 939.
(16) Cronkhite, J. M.; Stickel, R. E.; Nicovich, J. M.; Wine, P. H. *J. Phys. Chem. A* **1999**, *103*, 3228.
(17) Solomon, S.; Garcia, R. R.; Ravishankara, A. R. *J. Geophys. Res.* **1994**, *99*, 20491.
(18) Fahr, A.; Nayak, A. K.; Kurylo, M. J. *Chem. Phys.* **1995**, *197*, 195.
(19) Rattigan, O. V.; Shallcross, D. E.; Cox, R. A. *J. Chem. Soc., Faraday Trans.* **1997**, *93*, 2839.
(20) Roehl, C. M.; Burkholder, J. B.; Moortgat, G. K.; Ravishankara, A. R.; Crutzen, P. J. *J. Geophys. Res.* **1997**, *102*, 12819.
(21) Carl, S. A.; Crowley, J. N. *Atmos. Chem. Phys.* **2001**, *1*, 1.
(22) Cotter, E. S. N.; Canosa-Mas, C. E.; Manners, C. R.; Wayne, R. P.; Shallcross, D. E. *Atmos. Environ.* **2003**, *37*, 1125.

(23) Cotter, E. S. N.; Booth, N. J.; Canosa-Mas, C. E.; Shallcross, D. E.; Wayne, R. P. *Phys. Chem. Chem. Phys.* **2001**, *3*, 402.
(24) Cotter, E. S. N.; Booth, N. J.; Canosa-Mas, C. E.; Wayne, R. P. *Atmos. Environ.* **2001**, *35*, 2169.
(25) Wingenter, O. W.; Kubo, M. K.; Blake, N. J.; Smith, T. W., Jr.; Blake, D. R.; Rowland, F. S. *J. Geophys. Res.* **1996**, *101*, 4331.
(26) Spicer, C. W.; Chapman, E. G.; Finlayson-Pitts, B. J.; Plastridge, R. A.; Hubbe, J. M.; Fast, J. D.; Berkowitz, C. M. *Nature (London)* **1998**, *394*, 353.
(27) Ayhens, Y. V.; Nicovich, J. M.; McKee, M. L.; Wine, P. H. *J. Phys. Chem. A* **1997**, *101*, 9382.
(28) Bilde, M.; Wallington, T. J. *J. Phys. Chem. A* **1998**, *102*, 1550.
(29) Piety, C. A.; Nicovich, J. M.; Ayhens, Y. V.; Estupinan, E. G.; Soller, R.; McKee, M. L.; Wine, P. H. In Book of Abstracts; 14th International Symposium on Gas Kinetics, Leeds, UK, 1996.
(30) Bilde, M.; Sehested, J.; Nielsen, O. J.; Wallington, T. J.; Meagher, R. J.; McIntosh, M. E.; Piety, C. A.; Nicovich, J. M.; Wine, P. H. *J. Phys. Chem. A* **1997**, *101*, 8035.
(31) Goliff, W. S.; Rowland, F. S. *Geophys. Res. Lett.* **1997**, *24*, 3029.
(32) Enami, S.; Hashimoto, S.; Kawasaki, M.; Nakano, Y.; Ishiwata, T.; Tonokura, K.; Wallington, T. J. *J. Phys. Chem. A* **2005**, *109*, 1587.
(33) Orlando, J. J.; Tyndall, G. S. *J. Phys. Chem. A* **2002**, *106*, 312.
(34) Gilles, M. K.; Burkholder, J. B.; Gierczak, T.; Marshall, P.; Ravishankara, A. R. *J. Phys. Chem. A* **2002**, *106*, 5358.
(35) Piety, C. A.; Soller, R.; Nicovich, J. M.; McKee, M. L.; Wine, P. H. *Chem. Phys.* **1998**, *231*, 155.
(36) Finlayson-Pitts, B. J.; Pitts, J. N., Jr. *Chemistry of the Upper and Lower Atmosphere*; Academic Press: New York, 2000; p 146.
(37) Busch, G. E.; Mahoney, R. T.; Morse, R. I.; Wilson, K. R. *J. Chem. Phys.* **1969**, *51*, 449.
(38) Park, J.; Lee, Y.; Flynn, G. W. *Chem. Phys. Lett.* **1991**, *186*, 441.
(39) Tyndall, G. S.; Orlando, J. J.; Kegley-Owen, C. S. *J. Chem. Soc., Faraday Trans.* **1995**, *91*, 3055.
(40) Fletcher, I. S.; Husain, D. *Chem. Phys. Lett.* **1977**, *49*, 516.
(41) Chichinin, A. I.; Krasnoperov, L. N. *Chem. Phys. Lett.* **1989**, *160*, 448.
(42) Porret, D.; Goodeve, C. F. *Proc. R. Soc. London, Ser. A* **1938**, *165*, 31.
(43) Stated minimum purity of liquid phase in high-pressure cylinder.
(44) Shetter, R. E.; Davidson, J. A.; Cantrell, C. A.; Calvert, J. G. *Rev. Sci. Instrum.* **1987**, *58*, 1427.
(45) Orlando, J. J.; Tyndall, G. S.; Bilde, M.; Ferronato, C.; Wallington, T. J.; Vereecken, L.; Peeters, J. *J. Phys. Chem. A* **1998**, *102*, 8116.
(46) Yarwood, G.; Peng, N.; Niki, H. *Int. J. Chem. Kinet.* **1992**, *24*, 369.
(47) Waschewsky, G. C. G.; Horansky, R.; Vaida, V. *J. Phys. Chem.* **1996**, *100*, 11559.
(48) Seetula, J. A.; Gutman, D.; Lightfoot, P. D.; Rayes, M. T.; Senkan, S. M. *J. Phys. Chem.* **1991**, *95*, 10688.
(49) Knyazev, V. D.; Bencsura, A.; Dubinsky, A.; Gutman, D.; Melius, C. F.; Senkan, S. M. *J. Phys. Chem.* **1995**, *99*, 230.
(50) Frisch, M. J.; Trucks, G. W.; Schlegel, H. B.; Scuseria, G. E.; Robb, M. A.; Cheeseman, J. R.; Montgomery, Jr., J. A.; Vreven, T.; Kudin, K. N.; Burant, J. C.; Millam, J. M.; Iyengar, S. S.; Tomasi, J.; Barone, V.; Mennucci, B.; Cossi, M.; Scalmani, G.; Rega, N.; Petersson, G. A.; Nakatsuji, H.; Hada, M.; Ehara, M.; Toyota, K.; Fukuda, R.; Hasegawa, J.; Ishida, M.; Nakajima, T.; Honda, Y.; Kitao, O.; Nakai, H.; Klene, M.; Li, X.; Knox, J. E.; Hratchian, H. P.; Cross, J. B.; Bakken, V.; Adamo, C.; Jaramillo, J.; Gomperts, R.; Stratmann, R. E.; Yazyev, O.; Austin, A. J.; Cammi, R.; Pomelli, C.; Ochterski, J. W.; Ayala, P. Y.; Morokuma, K.; Voth, G. A.; Salvador, P.; Dannenberg, J. J.; Zakrzewski, V. G.; Dapprich, S.; Daniels, A. D.; Strain, M. C.; Farkas, O.; Malick, D. K.; Rabuck, A. D.; Raghavachari, K.; Foresman, J. B.; Ortiz, J. V.; Cui, Q.; Baboul, A. G.; Clifford, S.; Cioslowski, J.; Stefanov, B. B.; Liu, G.; Liashenko, A.; Piskorz, P.; Komaromi, I.; Martin, R. L.; Fox, D. J.; Keith, T.; Al-Laham, M. A.; Peng, C. Y.; Nanayakkara, A.; Challacombe, M.; Gill, P. M. W.; Johnson, B.; Chen, W.; Wong, M. W.; Gonzalez, C.; Pople, J. A. *Gaussian 03*, Revision B.4; Gaussian, Inc., Wallingford CT, 2004.
(51) Koch, W.; Holthausen, M. C. *A Chemist's Guide to Density Functional Theory*; Wiley: New York, 2001.
(52) (a) Bergner, A.; Dolg, M.; Küchle, W.; Stoll, H.; Preuss, H. *Mol. Phys.* **1993**, *80*, 1431. (b) Schwerdtfeger, P.; Dolg, M.; Schwarz, W. H.; Bowmaker, G. A.; Boyd, P. D. W. *J. Chem. Phys.* **1989**, *91*, 1762.
(53) G2: Curtiss, L. A.; Raghavachari, K.; Trucks, G. W.; Pople, J. A. *J. Chem. Phys.* **1991**, *94*, 7221.
(54) G2(MP2): Curtiss, L. A.; Raghavachari, K.; Pople, J. A. *J. Chem. Phys.* **1993**, *98*, 1293.
(55) Glukhovtsev, M. N.; Pross, A.; McGrath, M. P.; Radom, L. *J. Chem. Phys.* **1995**, *103*, 1878; Erratum *J. Chem. Phys.* **1996**, *104*, 3407.
(56) Chase, M. W., Jr.; Davies, C. A.; Downey, J. R., Jr.; Frurip, D. J.; McDonald, R. A.; Syverud, A. N. *J. Phys. Chem. Ref. Data* **1985**, *14* (Supplement I).
(57) (a) Gräfenstein, J.; Kraka, E.; Cremer, D. *Phys. Chem. Chem. Phys.* **2004**, *6*, 1096. (b) Fourré, I.; Bergès, J. *J. Phys. Chem. A* **2004**, *108*, 898. (c) Braïda, B.; Lauvergnat, D.; Hiberty, P. C. *J. Chem. Phys.* **2001**, *115*, 90. (d) Fourré, I.; Silvi, B.; Sevin, A.; Chevreau, H. *J. Phys. Chem. A* **2002**, *106*, 2561. (e) Braïda, B.; Thogersen, L.; Wu, W.; Hiberty, P. C. *J. Am. Chem. Soc.* **2002**, *124*, 11781. (f) Chermette, H. *J. Chem. Phys.* **2001**, *115*, 11068. (g) Braïda, B.; Hiberty, P. C. *J. Phys. Chem. A* **2000**, *104*, 4618. (h) Braïda, B.; Hiberty, P. C.; Savin, A. *J. Phys. Chem. A* **1998**, *102*, 7872. (i) Burda, J. V.; Hobza, P.; Zahradník, R. *J. Phys. Chem. A* **1997**, *101*, 1134.
(58) Benson, S. W. *Thermochemical Kinetics*; John Wiley & Sons: New York, 1968.
(59) Atkinson, R.; Baulch, D. L.; Cox, R. A.; Crowley, J. N.; Hampson, R. F., Jr.; Hynes, R. G.; Jenkin, M. E.; Kerr, J. A.; Rossi, M. J.; Troe, J. IUPAC Subcommittee for Gas Kinetic Data Evaluation; www.iupac-kinetic.ch.cam.ac.uk.
(60) Sander, S. P.; Friedl, R. R.; Ravishankara, A. R.; Golden, D. M.; Kolb, C. E.; Kurylo, M. J.; Huie, R. E.; Orkin, V. L.; Molina, M. J.; Moortgat, G. K.; Finlayson-Pitts, B. J. *Chemical Kinetics and Photochemical Data for Use in Atmospheric Studies*, Evaluation #14; JPL Publication 02-25; Jet Propulsion Laboratory, Pasadena, CA, 2003.
(61) Enami, S.; Ueda, J.; Goto, M.; Nakano, Y.; Aloisio, S.; Hasimoto, S.; Kawasaki, M. *J. Phys. Chem. A* **2004**, *108*, 6347.
(62) Orlando, J. J.; Tyndall, G. S.; Vereecken, L.; Peeters, J. *J. Phys. Chem. A* **2000**, *104*, 11578.
(63) Hasson, A.; Tyndall, G. S.; Orlando, J. J. *J. Phys. Chem. A* **2004**, *108*, 5979.
(64) Meagher, R. J.; McIntosh, M. E.; Hurley, M. D.; Wallington, T. J. *Int. J. Chem. Kinet.* **1997**, *29*, 619.
(65) Braun, W.; Herron, J. T.; Kahaner, D. K. *Int. J. Chem. Kinet.* **1988**, *20*, 51.
(66) Tomas, A.; Villenave, E.; Lesclaux, R. *J. Phys. Chem. A* **2001**, *105*, 3505.
(67) Veyret, B.; Lesclaux, R.; Rayez, M.-T.; Rayez, J. C.; Cox, R. A.; Moortgat, G. K. *J. Phys. Chem.* **1989**, *93*, 2368.
(68) Wine, P. H.; Semmes, D. H. *J. Phys. Chem.* **1983**, *87*, 3572.
(69) Donaghy, T.; Shanahan, I.; Hande, M.; Fitzpatrick, S. *Int. J. Chem. Kinet.* **1993**, *25*, 273.
(70) Tyndall, G. S.; Orlando, J. J.; Wallington, T. J.; Dill, M.; Kaiser, E. W. *Int. J. Chem. Kinet.* **1997**, *29*, 43.
(71) Shi, J.; Wallington, T. W.; Kaiser, E. W. *J. Phys. Chem.* **1993**, *97*, 6184.